Characterising regime behaviour in the stably stratified nocturnal boundary layer on the basis of stationary Markov chains

Carsten Abraham[1] and Adam H. Monahan[1]

[1]University of Victoria, School of Earth and Ocean Sciences, P.O. Box 3065 STN CSC, Victoria, BC V8P 5C2, Canada

Correspondence: Carsten Abraham (abrahamc@uvic.ca)

Abstract. Recent research has demonstrated that hidden Markov model (HMM) analysis is an effective tool to classify regimes of the stratified nocturnal boundary layer (SBL) at different tower sites. Here we analyse if SBL regime statistics (the occurrence of regime transitions, subsequent transitions after the first, and very persistent nights) in observations match theoretical calculations obtained from a stationary Markov chain with the goal of developing the foundations of novel Markov-chain-based boundary layer schemes which capture the effects of SBL regime dynamics. The regime statistics of a stationary Markov chain using the best estimate transition probabilities from the HMM analyses generally overestimate occurrence probabilities of regime transitions, resulting in an underestimation of persistent nights. Across the locations considered, sensitivity analyses of transition probability matrices in the HMM and the stationary Markov chain reveal that regimes are generally required to be more persistent in the stationary Markov chain in order to simulate observations accurately. A range of transition probability matrices allowing for a relatively accurate description of the occurrence of at least one transition within a night, multiple transitions, and the mean event durations is identified. The occurrence of very persistent nights (nights without regime transitions) is found to depend highly on the season. Therefore, for better representations of very persistent nights a nonstationary Markov chain linked to external drivers is likely appropriate. The observed transition probability maximum between one and two hours after a previous transition cannot be accounted for by two-state Markov processes (stationary or not). The use of these results in the development of SBL turbulence parameterisations is discussed.

1 Introduction

The stably stratified nocturnal boundary layer (SBL) can be classified into two distinct regimes, denoted the weakly and very stable boundary layers (respectively wSBL and vSBL, e.g. Mahrt, 1998a; Acevedo and Fitzjarrald, 2003; Mahrt, 2014; van Hooijdonk et al., 2015; Monahan et al., 2015; Vercauteren and Klein, 2015; Acevedo et al., 2016; Vignon et al., 2017; Abraham and Monahan, 2018a, b, c, hereafter AM18a, AM18b, and AM18c). The wSBL is characterised by weak stratification, strong wind, and sustained turbulence. The vSBL is characterised by strong stratification, low wind speeds, and collapsed turbulence where vertical coupling of the atmospheric layers weakens. Very stable boundary layers are also sometimes found to display so-called upside down turbulence, in which turbulence kinetic energy (TKE) is generated aloft by strong shears and then transported downwards. In this study we analyse how well the statistics of SBL regime occupation and regime transitions can

be described by two-regime Markovian system, with the ultimate goal of using this information to develop a new class of stoachstic parameterisations of the turbulence in the SBL in models of weather and climate.

In AM18a,b,c we have demonstrated that the hidden Markov model (HMM, section 3) analysis of Reynolds-averaged mean states can be used as a tool to systematically detect, diagnose, and analyse the SBL regimes at tower sites in many different

5 settings. Independent of the surface type, the climatological region, or the complexity of the surrounding topography, two distinct regimes in the state variable spaces of Reynolds-averaged mean states and turbulence have been found.

Over land, the wSBL to vSBL transition (the collapse of turbulence) is normally caused by radiative cooling at the surface increasing the inversion strength and suppressing vertical turbulent fluxes of momentum and heat. This process is relatively well understood and can be explained by conceptual models (van de Wiel et al., 2007, 2017; Holdsworth et al., 2016), or direct

10 numerical simulations of stratified channel flows (Donda et al., 2015; van Hooijdonk et al., 2017) or atmospheric boundary layers (e.g. Flores and Riley, 2011; Ansorge and Mellado, 2014). Radiative cooling leads to very shallow boundary layers for which vertical resolution of large-scale circulation models is usually not sufficient for accurate simulation. Over oceans, the wSBL to vSBL transition is found to be caused by the advection of warm air aloft (AM18b,c) producing vSBL conditions which are not as shallow as over land.

15 The reverse transition, the recovery of turbulence (vSBL to wSBL transition) is less well-understood. Mechanisms by which turbulence recovers include the build-up of shear resulting in instabilities, or an increase in cloud cover weakening the stratification through increasing the downwelling longwave radiation (AM18c). Another potential class of processes initiating these transitions is associated with intermittent turbulent events (e.g. Mahrt, 2014, and references within) which have been found to dominate the turbulent transport in vSBL conditions (Nappo, 1991; Coulter and Doran, 2002; Doran, 2004; Basu et al.,

20 2006; Acevedo et al., 2006; Williams et al., 2013). Intermittent turbulence arises from a range of different phenomena such as breaking gravity waves or solitary waves (Mauritsen and Svensson, 2007; Sun et al., 2012), density currents (Sun et al., 2002), microfronts (Mahrt, 2010), Kelvin-Helmholtz instabilities interacting with the turbulent mixing (Blumen et al., 2001; Newsom and Banta, 2003; Sun et al., 2012), or shear instabilities induced from internal wave propagation (Sun et al., 2004; Zilitinkevich et al., 2008; Sun et al., 2015). It has also been suggested from direct numerical simulations that intermittency can arise as an

25 intrinsic mode of the non-linear equations in the absence of external perturbations of the mean flow (Ansorge and Mellado, 2014). Regardless of which process causes the recovery of turbulence, all phenomena are subgrid-scale in the state-of-the-art weather and climate models and are typically not included through explicit process-based parameterisations.

Although processes in the SBL have been extensively studied, substantial errors of SBL representation persist in weather and climate models (Dethloff et al., 2001; Gerbig et al., 2008; Bechtold et al., 2008; Medeiros et al., 2011; Kyselý and Plavcová,

30 2012; Tastula et al., 2012; Sterk et al., 2013; Bosveld et al., 2014; Sterk et al., 2015). Misrepresentation of the SBL includes unrealistic decoupling of the atmosphere from the surface resulting in runaway surface cooling (Mahrt, 1998b; Walsh et al., 2008), underestimation of the wind turning with height within the boundary layer (Svensson and Holtslag, 2009), overestimation of the boundary layer height (Bosveld et al., 2014), underestimated low level jet speed (Baas et al., 2009), and underestimation of near-surface wind speed and temperature gradients or their diurnal cycle (Edwards et al., 2011).

Accurate simulations of these near-surface properties is particularly important for global and regional weather forecasts of vertical temperature structures, for instance, which control the formation of fog and frost (Walters et al., 2007; Holtslag et al., 2013). More accurate simulations of the SBL regime behaviour are also important for better representations of surface wind variability and wind extremes (He et al., 2010, 2012; Monahan et al., 2011); simulation and assessment of pollutant dispersal,

5   air quality (Salmond and McKendry, 2005; Tomas et al., 2016), and harvesting of wind energy (Storm and Basu, 2010; Zhou and Chow, 2012; Dörenkämper et al., 2015); and agricultural forecasts (Prabha et al., 2011; Holtslag et al., 2013).

Global and regional weather and climate models often use an artificially enhanced surface exchange under stable conditions in order to improve simulations of the large-scale flow (Holtslag et al., 2013). This approach has led to the introduction of long-tailed stability functions not justifiable by observations. In such models, turbulence is artificially sustained under very

10   stable conditions and the two-regime characteristic of the SBL is suppressed, biasing near surface winds and temperature profiles. Without this parameterisation the nocturnal boundary layers can experience a single turbulence collapse which persists for the entire night. Although the long-tailed stability functions in relatively coarse-resolution models mimic to some extent the grid box effect of the two-regime structure, with increasing horizontal and vertical resolution more accurate process-based parameterisations are necessary. The vSBL to wSBL transition does not demonstrate clear precursors in internal or

15   external state variables (AM18c), indicating that parameterisations of the effects of these kinds of transitions in weather and climate models may be required to be explicitly stochastic (e.g. He et al., 2012; Mahrt, 2014). In particular, phenomena such as intermittent turbulence events will likely rely on stochastic parameterisations as their structure and propagation are found to be only weakly-dependent on the mean states (e.g. Rees and Mobbs, 1988; Lang et al., 2018). Stochastic subgrid-scale parameterisations to describe the physically different conditions in the SBL have been proposed to help capturing the

20   missing variability in the SBL and improve both climate mean states and forecast ensemble spread (e.g. He et al., 2012; Mahrt, 2014; Nappo et al., 2014; Vercauteren and Klein, 2015). One possible approach to developing a stochastic parameterization of turbulence with the ability to simulate regime transitions is to use the transition probability matrices estimated by the HMM (AM18a). The HMM analyses presented in AM18a, however, assumes stationary regime dynamics. In AM18b and AM18c clear evidence of nonstationarities was found, such as an elevated probability of turbulence collapse during sunset linked to the

25   diel cycle and or seasonally-varying probabilities of very persistent nights.

As a first approach to establishing a foundation of a stochastic parameterisation of turbulence in the SBL, we first analyse in this study how well a stationary Markov chain can characterize the observed regime statistics. Subsequently, we present the sensitivity of the regime sequence estimated by the HMM to the perturbations of the persistence probabilities in order to quantify what ranges of persitence probabilities describe regime statistics in SBL observations accurately. Comparing this

30   sensitivity analysis with a sensitivity analysis of regime statistics to varying persistence probabilities in a stationary Markov chain we quantify what range of persistence probabilities are consistent with the observations and simulated SBL regime statistics. The study is organised as follows. First a very short review of the observational data used in the HMM analysis is given in section 2, followed by a brief review of the HMM application to the SBL (section 3). Results are shown in section 4 and a discussion and conclusions in section 5.

2 Data

The observational data used in this study have been discussed in detail in AM18(a,b,c). We present here a short summary of the data. Observational data sets from eight different research towers measuring standard Reynolds-averaged meteorological state variables with a time resolution of 30 minutes or finer are considered (Table 1). The observational levels of wind speeds and

5   temperatures correspond to the reference state variable set determined in AM18a (Table 1). Substantial differences among the eight experimental sites exist in terms of their surface conditions, surrounding topography, and their typical synoptic patterns. As a simple classification scheme, we distinguish between land-based and ocean-based stations.

The land-based stations can be further clustered into different subsets. Both the Cabauw and Hamburg towers lie in flat, humid, grassland areas, although the Hamburg tower is affected by the large metropolitan area of Hamburg. The Karlsruhe

10   tower is located in the Rhine valley, a rather hilly, forested area in the lee of an urban area. The American sites, Boulder and Los Alamos, are strongly affected by the surrounding topography of the Rocky Mountains.

The ocean-based stations are the offshore research platforms *Forschungsplattform in Nord- und Ostsee* (FINO) which are located in the German Northern and Baltic Seas. These sites are characterized by relatively homogeneous local surroundings and a large surface heat capacity. At the FINO towers we exclude nights with statically unstable conditions (defined as nights

15   with two or more unstable datapoints in a night) as under these conditions at the wind speed measurements have been found to be unreliable (Westerhellweg and Neumann, 2012). Furthermore, at FINO-1 nights with primary wind directions between 280 and 340 degrees are excluded due to mast interference effects in the data. At the other stations such an exclusion is not necessary as three wind measurements with 120 degree separation are taken at each level.

3 Brief summary of the hidden Markov model

20   We now present a brief overview of the HMM analysis with application to the SBL (Monahan et al., 2015, AM18a). An in-depth description of HMM analysis can be found in Rabiner (1989) and an illustrative example is given in Monahan et al. (2015).

We use the HMM to systematically detect and characterize regime behaviour in the SBL from observed data. The HMM assumes that underlying the observations is an unobserved, or hidden, discrete Markov chain ($\mathbf{X} = \{x_1, x_2, \ldots, x_T\}$). The

25   analysis estimates the regime-dependent parametric probability density distributions of the observations, the transition matrix $\mathbf{Q}$ associated with X, and a most likely regime path of the Markov chain (known as the Viterbi Path, VP). We associate the different states of the Markov chain with the SBL regimes (wSBL and vSBL). In our analysis we use observations of the three-dimensional vector consisting of the Reynolds-averaged vertically-averaged mean wind speed, wind speed shear, and stratification to define the HMM input vector $\mathbf{Y}$. A detailed justification of this observational input dataset is presented in

30   AM18a. The HMM estimation algorithm makes use of the following assumptions:

1. Markov assumption: the regime occupation x_{t+1} depends exclusively on the current regime of x_t, so:

$$P(x_{t+1} = i | x_t = j, x_{t-1} = k, \ldots, x_0 = n) = \mathbf{Q_{ij}} P(x_t = j) \qquad \forall t, \tag{1}$$

where the dynamics of the SBL are governed by $\mathbf{Q}$ (a 2×2 matrix corresponding to the wSBL and vSBL, respectively) such that $\sum_i \mathbf{Q_{ij}} = 1$.

2. Independence assumption: conditioned on $\mathbf{X}$, values of $\mathbf{Y}$ are independent and identically distributed variables resulting in a probability of the observational data sequence of

$$P(\mathbf{Y}|\mathbf{X},\lambda) = \pi_j p(\mathbf{y}_1|x_1 = j, \lambda_j) \prod_{t=2}^{T} \mathbf{Q_{ij}} p(\mathbf{y}_t|x_t = i, \lambda_i) \qquad \text{with} \quad i,j = 1,\ldots,K, \tag{2}$$

where $\{\lambda_i\}_{i=1}^{K}$ is the parameter set describing the probability distribution (taken to be Gaussian mixture models as in AM18a) of $\mathbf{y_t}$ conditioned on the regime i or j of x_t (wSBL or vSBL), and π_j is the probability that x_1 is in regime j.

3. Stationarity: this analysis assumes that $\mathbf{Q}$ and λ are time-independent.

The goal of the HMM analysis is to estimate the full set of parameters $\Lambda = \{\lambda_i, \pi_i, \mathbf{Q}\}$ from $\mathbf{Y}$. Starting from the probability of the observational time series conditioned on the parameters $P(\mathbf{Y}|\Lambda)$ and applying Bayes theorem to obtain $P(\Lambda|\mathbf{Y})$, the problem reduces to a maximum-likelihood estimation which can be iteratively solved to find local maxima via the expectation maximisation algorithm (Dempster et al., 1979). Having estimated Λ, the most likely regime sequence (the VP) can be calculated. The estimation of the parameters in the expectation-maximisation scheme for our analysis is described in detail in Rabiner (1989).

One limitation of the HMM model considered is that it assumes stationary statistics, However, nonstationarities linked to the diel cycle and seasonal variability are present in the regime statistics of the SBL (cf. next section, AM18b, AM18c). Generalizations exist which can account for nonstationarities, such as nonhomogeneous HMMs (Hughes et al., 1999; Fu et al., 2013). We chose to consider stationary HMM analysis in this study in order to investigate the simplest possible approach to a stochastic parameterisation of the turbulence under SBL conditions. With this approach we can assess the potential of such relatively simple parameterisation and identify where extra complexity is warranted.

4   Results

In order to base new parameterisations of turbulence in the SBL on stationary Markov chains such as are produced by the HMM, it is important that these model the observed regime statistics accurately. Here, we analyse how well a stationary Markov chain (using the best-fit transition matrix $\mathbf{Q}_{\mathrm{ref}}$ from the HMM analysis in AM18a; Table 1) can model SBL regime statistics (event durations and the probabilities of very persistent nights, of any transition occurrences within a night, and of multiple transition occurrences within a night) as found in AM18b and AM18c. Repeating the HMM analysis using a specified $\mathbf{Q}$ held fixed at values other than $\mathbf{Q}_{\mathrm{ref}}$, we then investigate the sensitivity of the estimated regime statistics of these perturbed VPs relative to the reference VP from $\mathbf{Q}_{\mathrm{ref}}$ (VP$_{\mathrm{ref}}$). Finally, we vary $\mathbf{Q}$ to assess if persistence probabilities exist that match SBL statistics in both theoretical calculations using a stationary Markov chain and in observations. The mathematical expressions used to compute the statistics of interest from the HMM transition matrices are presented in the Appendix.

4.1 Comparison of observations and stationary Markov chain calculations

As described in AM18b, the occurrence of very persistent nights varies with the duration of the night in a manner consistent with the influence of seasonal changes in large-scale meteorological conditions (respectively higher and lower probabilities of the wSBL and vSBL in wintertime; Figure 1). Using $\mathbf{Q}_{ref}$ (based on data from all seasons), we can compute theoretical

5 probabilities of the occurrence of persistent SBL nights in a stationary Markov chain (c.f. eq. A1 and A2) against which we can compare the observed relative frequencies for different lengths of nights. As the tower sites are located in the midlatitudes seasonal changes lead to nighttime duration changes between 8 to 15 hours (at 45 N) between summer and winter.

For a stationary Markov chain, the frequency of the occurrence of persistent wSBL nights decreases monotonically with the length of the night. The probabilities of very persistent wSBL nights in summer (of duration 8 to 10 hours) agree rela-

10 tively well with the theoretical calculations (Figure 1). However, for the longer duration nights the stationary Markov chain underestimates the occurrence of persistent wSBL nights as the observed probabilities increase rather than decrease. The increase of wSBL probability with length of night is consistent with larger synoptic-scale variability (with stronger mechanical generation of turbulence) in the winter, but not consistent with a stationary Markov chain. The observed probability of very persistent vSBL nights decreases with increasing length of the night, consistent with the increase in mean pressure gradient

15 force. While the stationary Markov chain also shows this behaviour, it systematically underestimates the observed occurrence of very persistent vSBL nights. Furthermore, the non-stationary change in synoptic driving is not embedded in the stationary Markov chain.

In AM18c we have shown that the probability of at least one wSBL to vSBL transition (including nights in which the first wSBL to vSBL transition follows an initial one from the vSBL to the wSBL) occurring within a night shows no systematic

20 dependence of the length of the night across the tower sites (Figure 2). At most land-based stations the probability of occurrence slightly decreases, with the exception of Cabauw where the probability slightly increases. At ocean-based stations the probability of the occurrence of wSBL to vSBL transitions is not systematically sensitive to the length of the night. The probability of the occurrence turbulence recovery events is also insensitive to the season. In contrast, the occurrence probability of at least one transition obtained from the stationary Markov chain (Eqns. A3 and A4) increases with the length of the night, and

25 is larger than those of observations at all sites (Figure 2, lower panels). The overestimation of turbulence recovery events by the stationary Markov chain is slightly larger than that of turbulence collapse events at land-based stations, while the opposite is true at ocean-based stations.

The occurrence of a recovery event subsequent to a turbulence collapse is better estimated by a stationary Markov chain (Eqns. A6 and A8, Figure 3) than the overall occurrence of a at least one wSBL to vSBL transition (Figure 2, left panels).

30 Both observed and modelled probabilities increase with the length of the night, at about the same rate. Interestingly, at land-based stations fewer subsequent turbulence recovery events are observed than expected, and over oceans more are observed. The distributions of turbulence collapse events subsequent to a recovery event theoretical calculations of the Markov chain are generally close to the observations in summer and worsen slightly for winter conditions (Figure 3, right panels).

Nonlinear Processes
in Geophysics
Discussions

The occurrence of subsequent transition events can be also associated with event durations in the vSBL (subsequent recovery event) and wSBL (subsequent collapse event). The observed mean event vSBL durations are generally close to the theoretical values obtained from the stationary Markov chain for nights of all durations between 8 and 15 hours (Figure 4). While agreement is reasonably good for wSBL events, the stationary Markov chain generally underestimates the mean duration. In

5 AM18c we demonstrated that the probability density functions (pdfs) of the time between successive transitions show very similar structures for wSBL and vSBL event durations (Figure 5). Interestingly, these pdfs display clear maxima between one and two hours after the preceding transition, demonstrating that the occurrence of subsequent transitions most often requires some relaxation time. These recovery periods following the transitions cannot be accounted for by the stationary two-regime Markov chain we consider. The theoretical duration pdfs of events for nights lasting from 8 to 15 hours (equations A5 and A7)

10 decay monotonically. The probabilities of subsequent transition occurrence after about 2 hours are similar in the theoretical stationary Markov chain and the observations.

The results above demonstrate the existence of at least two aspects of the regime statistics which cannot be accounted for by a two-regime stationary Markov chain. First, the occurrence of very persistent regimes and (to lesser extent) the occurrence of transitions are subject to non-stationary seasonal changes. Accounting for these nonstationarities would require

15 seasonally-varying persistence probabilities or (more naturally) persistence probabilities that depend on seasonally-varying external parameters. Such behaviour could potentially be represented by a non-homogeneous HMM (e.g Hughes et al., 1999; Fu et al., 2013). Note that these results do not invalidate the use of the HMM for classification purposes, as the VP is only weakly sensitive to $\mathbf{Q}$ (as will be shown in the next section). Second, the maximum in event duration pdfs one to two hours after the preceding transition is inconsistent with the statistics of a two-regime Markov chain. Nonetheless, results indicate that

20 even though the occurrence probability of the first transition in the night by the stationary Markov chain is biased, once the first transition has occurred a stationary Markov chain is able to predict the general occurrence of subsequent transitions and their mean regime duration. Due to the fact the values on the diagonal of $\mathbf{Q}_{\mathrm{ref}}$ are close to one (Table 1), theoretical regime statistics calculated from the from the stationary Markov chain are sensitive to these values (cf. Eqns. A1-A8). In contrast, the estimated VP has a weak sensitivity to the those elements of $\mathbf{Q}$. We now turn to these sensitivity analyses.

25 ## 4.2 Sensitivity of the VP to perturbed persistence probabilities

We consider the sensitivity of the VPs to changes of the persistence probabilities in $\mathbf{Q}$ by holding this matrix fixed and repeating the HMM analysis. We will show that there is a relatively large range of persistence probabilities in which the perturbed VPs are in high agreement with $\mathrm{VP}_{\mathrm{ref}}$. These ranges of persistence probabilities could then be appropriate to inform a two-regime stochastic parameterisation of SBL turbulence. In order to assess if the perturbed VPs are consistent with $\mathrm{VP}_{\mathrm{ref}}$ we consider

30 first the overall consistency between the two (fraction in which both VPs are in the same regime). Similar as in AM18a, we then assess the consistency of the timing of transitions (simultaneity of transitions in the reference and perturbed VPs) as well as the representation of very persistent nights to obtain the total VP consistency. For this part of the analysis, we focus on the Cabauw tower data as we have analysed these data extensively in AM18a. The same qualitative results are found using all tower station data we have considered (not shown).

The VP of the HMM model is robust to quite substantial changes in $\mathbf{Q}$, with an overall accuracy of more than 90 % obtained for ranges of wSBL and vSBL persistence probabilities between 0.5 and about 0.9999 (Figure 6, upper left panel). Agreement at the 99 % level is found for persistence probabilities between approximately 0.9 and 0.9999. Accurate representation of the timing of transitions is found for a broad range of low persistence probabilities and a small range of persistence probabilities

5 spanning approximately from 0.96 to 0.99. Evidently, if both persistence probabilities are below 0.5 (regime transitions in a single step are more probable than remaining in the regime) the accuracy of the transitions is above 99 %. However, this result is a consequence of the high frequency of modelled transitions improving the ability to capture individual observed transitions (at the expense of modelling far too many transition events). Because regime transitions are relatively rare, the physically meaningful range of persistence probabilities corresponds to relatively large values of both. The accuracy of the occurrence of

10 persistent wSBL nights in the perturbed VP is best for high $P(\text{wSBL} \rightarrow \text{wSBL})$ and is weakly sensitive to $P(\text{vSBL} \rightarrow \text{vSBL})$. This result is not surprising as the high wSBL persistence probability ensures that the majority of very persistent wSBL nights are captured. This measure is unaffected by any underestimate of the occurrence of persistent vSBL nights. Complimentary results are found for the occurrence of persistent vSBL nights.

Each of the five consistency measures illustrated in Figure 6 capture distinct aspects of agreement between the reference and

15 perturbed VPs. We define a good total consistency relative to VP_{ref} as each of the five described VP consistencies exceeding 99 %. At Cabauw, a 99 % total consistency can be achieved for $P(\text{wSBL} \rightarrow \text{wSBL})$ between approximately 0.97 and 0.99 and $P(\text{vSBL} \rightarrow \text{vSBL})$ between 0.98 and 0.99 (Figure 7). Figure 7 also depicts the ranges of persistence probabilities for which all five criteria exceed 95 %. If only a 95 % total VP consistency is required, $P(\text{wSBL} \rightarrow \text{wSBL})$ and $P(\text{vSBL} \rightarrow \text{vSBL})$ can range approximately between 0.95 and almost 1.

20 In AM18a a set of different transition matrices $\mathbf{Q}$ were estimated from HMM analyses of different state variable inputs: surface data such as friction velocity, surface pressure tendencies, and surface radiative fluxes; stratification; shear; turbulence variables such as TKE and vertical turbulent fluxes; and all combinations of these at different measurement altitudes. Most of these $\mathbf{Q}$ estimates fall within the 95 % total VP consistency levels (Figure 7). That the best agreement with the reference HMM is found for HMM analyses with state variable inputs including turbulence information (at any measurement height, and with

25 or without combinations of shear and stratification information) is not surprising as the two regimes distinguish the turbulent wSBL from the (essentially) non-turbulent vSBL. Outliers in the $\mathbf{Q}$ estimates using turbulence data come from state variable input vectors combining surface data such as the surface pressure with the near surface TKE. Highly consistent estimates of $\mathbf{Q}$ are obtained from combinations of shear and stratification, as these state variables describe the competing mechanisms of turbulence production and consumption and are used in the reference HMM. Interestingly, with respect to $\mathbf{Q}_{\text{ref}}$ the HMM

30 analyses of shear information alone tend to estimate larger persistence probabilities of regimes than those using stratification information alone. Less agreement is found for $\mathbf{Q}$ estimated from either stratification or shear information aloft without near-surface information (yellow and green dots outside of the 95 % total VP consistency level in Figure 7, cf. AM18a). These results demonstrate that the regime information is carried in a broad range of state variables.

The sensitivity analysis of the estimated regime occupation sequence to changes in $\mathbf{Q}$ values reveals that reasonably accurate

35 regime statistics can be obtained over a relatively large range of persistence probabilities. We will now repeat the sensitivity

analysis for the theoretical regime statistics of the stationary Markov chain to assess if a range of persistence probabilities exists where observed and modelled statistics are consistent. Such an analysis shows how well the SBL regime statistics can be approximated by a stationary two-regime Markov chain.

4.3 Sensitivity of SBL regime statistics to changing persistence probabilities in a stationary Markov chain

5 Calculation of the theoretical values of SBL regime statistics from a stationary Markov chain requires specifying the duration of the night (cf. Figures 1 to 4). For simplicity, we compare theoretical and observed regime statistics for three durations representative of individual seasons (Tables 2 and 3). The statistics considered include the individual probabilities of starting the night in the wSBL or vSBL (respectively π_{wSBL} and π_{vSBL}). While these probabilities of initial regimes do not affect the HMM analyses (not shown) they can have a substantial impact on the theoretical calculations in a stationary Markov chain.

10 This dependence is illustrated in Figure 8, which shows the sets of persistence probabilities for which the probability of at least on wSBL to vSBL transition (upper row) or reverse transition (middle row) from the stationary Markov chain matches the observed values, for a range of different values of π_{wSBL} and π_{vSBL}. Also shown are the isolines of total consistency of perturbed VP and VP$_{\text{ref}}$ from Figure 7 (grey lines). Depending on the values of π_{wSBL} and π_{vSBL}, large parts of the persistence probability curves fall within the range of persistence probabilities in which perturbed VPs are in good agreement with VP$_{\text{ref}}$.

15 Furthermore, for a range of π_{wSBL} and π_{vSBL} values, the lines corresponding to at least one of each transition intersect in a region of high total agreement of the perturbed and reference VP. For other ranges of π_{wSBL} and π_{vSBL}, no such intersections occur. However, the persistence probabilities needed in a stationary Markov chain to match occurrence probabilities of very persistent nights span a range of persistence probabilities well outside the contours for the 95 % total VP consistency of the perturbed VP (Figure 8, lower row). Persistence probabilities which ensure the right observational occurrence probability of

20 persistent nights and are closest to the range of perturbed VP consistency with VP$_{\text{ref}}$ are given for π_{wSBL} between 40 % to 60 %. These results are relatively insensitive to the season.

As demonstrated in the previous section the persistence probabilities ensuring good total VP consistency are relatively broad. We will now evaluate the range of persistence probabilities in a stationary Markov chain which is consistent with the observed persistence probabilities across all tower sites discussed in section 4.1. In order to account sampling variability in the observed

25 regime statistics and the effects of changes in π_{wSBL} we consider occurrence probabilities in an arbitrary 10 % error range ($\pm$ 5 %) around the values from VP$_{\text{ref}}$. In the following Figures the solid, dashed, and dotted lines respectively correspond to the reference, 5% decreased, and 5 % increased observational occurrence probabilities of at least one transition in a night (wSBL to vSBL in red; vSBL to wSBL in black). The range of persistence probabilities for which the stationary Markov chain models the observed occurrence probabilities of very persistent nights with 10 % uncertainties is displayed by a shaded

30 rectangle with **Q** with a mark for the exact observation. As in previous Figures isolines of total consistency of perturbed VP to VP$_{\text{ref}}$ are depicted in grey lines.

Similar to what was found at Cabauw, across all land-based stations the perturbed VP is not very sensitive to the values of **Q** and a relatively broad range of persistence probabilities allows for a 95 % total VP consistency in the HMM analyses (Figure

9). The persistence probabilities corresponding to the most likely VPs are reasonably similar across the different stations, with regime persistence probabilities between 0.95 and 0.99.

At almost all stations, the persistence probability values for which the stationary Markov chain regime transition statistics match the observed values fall outside the region of high total VP consistency between the reference and perturbed VPs (Figure 9). This fact is true for all seasons. Only at Cabauw do these ranges of persistence probabilities coincide fairly well. With the exception of Boulder and summertime in Los Alamos, the persistence probabilities in the stationary Markov chain needed to capture the observed regime transition statistics exceed those of the VP. This fact is consistent with the underestimation of occurrence probabilities of transitions by stationary Markov chains using $\mathbf{Q}_{\mathrm{ref}}$ shown in Figure 2.

As discussed in section 4.1 and AM18b, the probability of very persistent nights varies more with season than the occurrence of transitions (cf. Table 3 and Figure 1). This result is reflected in the fact that the range of persistence probabilities capturing the right regime transition statistics in a stationary Markov chain changes less dramatically between seasons than the optimal value to capture the occurrence probabilities of persistent nights (Figure 9). Only at Cabauw in wintertime and Hamburg in spring or autumn we can identify a range of persistence probabilities for the stationary Markov chain which is able to model all SBL regime statistics accurately within our imposed uncertainty range. At all other times and stations such a common range of persistence probabilities is generally absent. Similar to the occurrence probability of regime transitions, the exact occurrence probability of very persistent nights can only be modelled in a stationary Markov chain with higher persistence probabilities than the $\mathbf{Q}$ directly estimated from observations (with the exception of summertime at Cabauw and Karlsruhe where $P(\mathrm{wSBL} \rightarrow \mathrm{wSBL})$ has to be slightly smaller than $\mathbf{Q}_{\mathrm{ref}}$). Again this result is consistent with the general underestimation of occurrence probabilities of very persistent nights in a stationary Markov chain illustrated in Figure 11.

In almost all cases, the range of persistence probabilities accounting for uncertainties in the occurrence of very persistent nights includes the occurrence probability of one type of regime transitions. The statistics of turbulence recovery events and very persistent nights most often correspond to the same ranges of persistence probabilities than statistics of turbulence collapses with very persistent nights. Very rarely do these overlapping ranges of persistence probabilities also fall in the range persistence probabilities ensuring a good agreement between $\mathrm{VP}_{\mathrm{ref}}$ and perturbed VPs.

At ocean-based stations the range of persistence probabilities that ensures good agreement between the $\mathrm{VP}_{\mathrm{ref}}$ and the perturbed VPs is substantially larger than for land-based stations (Figures 10 and 11). The total VP consistency exceeds 95 % for regime persistence probabilities ranging from approximately 0.92 to 0.99. Similar to land based stations, the range of persistence probabilities for which both kinds of transitions agree well with the stationary Markov chain lies generally at larger persistence probabilities than values assuring good agreement between the reference and perturbed VPs. Only in winter do the persistence probabilities for which the stationary Markov chain captures the observed persistence probabilities fall below $\mathbf{Q}_{\mathrm{ref}}$ for $P(\mathrm{wSBL} \rightarrow \mathrm{wSBL})$ and above $\mathbf{Q}_{\mathrm{ref}}$ for $P(\mathrm{vSBL} \rightarrow \mathrm{vSBL})$. These results do not have a simple relationship to the underestimation of occurrence of transitions illustrated in Figure 12 as both persistence probabilities are important to calculate the occurrence probability of at least one transition (cf. A3 and A4). The agreement between observed and modelled occurrence probabilities of at least one transition is better at FINO-2 and FINO-3. For each season at these two sites, the region of persistence probabilities needed to capture the occurrence of at least one transition in a night in a stationary Markov chain

is much closer to $\mathbf{Q}_{\mathrm{ref}}$ than is the case for land-based stations. This result might be related to the fact that while our analysis has accounted to some degree for seasonal nonstationarities it has not allowed for diel nonstationarities. Over the oceans diel nonstationarities are substantially weaker than over land (cf. AM18c), where there is a pronounced maximum in the probability of wSBL to vSBL transitions occurring during sunset.

5   With the exception of FINO-1 the ocean-based stations show that a range of persistence probabilities can be identified in a stationary Markov chain for which all considered regime statistics match observations. These values tend to be in ranges of persistence probabilities exceeding 0.99. These values are considerably different from those found at land-based stations. This fact agrees well with the findings in AM18b and AM18c that transitions are radiatively-driven over land but advectively-driven over oceans. A result of these different mechanisms is a much lower occurrence of transitions and therefore higher frequency

10   of persistent nights over oceans. Nonetheless, the appropriate range of persistence probabilities capturing the regime statistics in a stationary Markov chain lie outside of the isolines where good agreement between reference and perturbed VPs is found.

As discussed in section 4.1, the occurrence of subsequent transitions and the event durations can be explained relatively well by a stationary Markov chain using $\mathbf{Q}_{\mathrm{ref}}$. In fact, we find that the statistics of subsequent transitions are simulated well over the whole range of persistence probabilities corresponding to a 95 % total VP accuracy in perturbed VPs (not shown). This result

15   reinforces the fact that once the first transition is captured or simulated many aspects of SBL regime statistics are modelled well by a stationary Markov process.

5   Discussion and Conclusions

Recent studies have demonstrated that hidden Markov model (HMM) analysis is an effective tool to classify the nocturnal boundary layer (SBL) into weakly stable (wSBL) and very stable (vSBL) conditions (Monahan et al., 2015, AM18a, AM18b,

20   AM18c). Due to the fact that weather and climate models are unable to accurately simulate SBL regime dynamics, the goal of this study is to investigate how this stationary two-regime Markov chain could be used as the foundation of new stochastic parameterisations for turbulence in the SBL. We have assessed the performance of the stationary Markov chain relative to the observed probabilities event durations and of the occurrences of very persistent nights (nights without SBL regime transitions), of any regime transitions, and of multiple subsequent transitions.

25   The observed occurrence of very persistent wSBL (vSBL) nights increases (decreases) from summer to winter, likely due to changes in the mean large-scale forcing between these seasons in the midlatitudes which are not accounted for by the stationary Markov chain. Using the HMM persistence probabilities the occurrence of regime transitions is overestimated by the stationary Markov chain. However, the modelled occurrence of transitions subsequent to a preceding one and the mean event durations in each regime are relatively close to observations across all sites and seasons. The event duration probability density functions

30   (pdfs), on the other hand, display a maximum an hour or two after sunset. Such a recovery time between regime transitions (AM18c) is not explainable by any stationary two-regime Markov chain. However, after these two hours event duration pdfs can be very well approximated by a stationary Markov chain.

By fixing the persistence probability matrix and producing new perturbed HMM regime sequences we have quantified the range of persistence probabilities that are consistent with the most likely HMM regime sequence. Across all land-based sites similar ranges of persistence probabilities are appropriate to describe the regime statistics of the SBL. The persistence probabilities estimated by HMM analyses using other observed state variables generally also fall into this range. This result

5   reinforces the findings of AM18a that the regime statistics are evident in many near-surface state variables. Across ocean-based sites the range of persistence probabilities that allows for accurate perturbed regime sequences is larger than at land-based sites.

The result that broadly the same range of persistence probability values describes the SBL regime statistics across tower sites indicates that a stochastic parameterisation based on the two-state Markov chain does not require parameters tuned to the fine details of local conditions. Systematic differences do exist between land- and ocean-based stations due to the different

10 mechanisms of transitions (AM18b, AM18c).

An analysis of the ranges of persistence probabilities for which a 'freely-running' stationary Markov chain is consistent with the observed regime transition statistics indicated that these generally exceed the values obtained from the HMM analysis. At ocean-based stations we find a better agreement between ranges of appropriate persistence probabilities in a stationary Markov chain and in observations. This result may be related to the fact that diel nonstationarities are weaker over oceans than over land

15 (cf. AM18c). As with the regime statistics for the occurrence of transitions, the occurrence probabilities of persistent nights can only be simulated in a stationary Markov chain with larger persistence probabilities than estimated from observations. In general, no range of persistence probabilities can be identified that is consistent with both the occurrence probabilities of both transitions and very persistent nights. The results indicate that the occurrence of very persistent nights cannot be accurately simulated by the same stationary Markov chain which is appropriate to capture the statistics of regime transitions because the

20 different classes of nights (with and without transitions) depends on the large-scale synoptic conditions.

Our results have direct relevance to the representation of SBL regimes in weather and climate models. The regime statistics show clear evidence of nonstationarity and non-Markov behaviour. These facts, and the fact that aspects of regime transitions such as radiatively-driven turbulence collapse can be simulated by models, indicate the need for state-dependent transition probabilities in any explicitly stochastic representation of SBL regime transitions.

25 We now discuss the form that such an explicitly stochastic parameterisation might take. State-of-the-art boundary layer turbulence parameterisations in weather and climate models are generally able to produce turbulence collapses during the nocturnal transition. However, the models do not correctly simulate turbulence recovery events as for instance intermittent turbulence events are not explicitly resolved. To overcome the resulting grid-box mean errors long-tailed stability function under stable conditions have been used causing turbulence never to collapse (e.g. Holtslag et al., 2013). A process-based

30 stochastic parameterisation, on the other hand, could simulate turbulence recovery events by driving the SBL episodically into a turbulence active regime (e.g He et al., 2012). Such turbulence impulses can be interpreted as being related to intermittent turbulence events. As in He et al. (2012), this stochastic forcing can be implemented as an extra source term in the turbulence kinetic energy (TKE) budget.

The stochastic parameterisation would use a new local variable tracking the SBL regime (wSBL or vSBL). At each time

35 step, the occurrence of a transition would be determined randomly using instantaneous state-dependent transition probabilities.

For instance, $P(\mathrm{wSBL} \rightarrow \mathrm{vSBL})$ could depend on the Richardson-number (Ri) in such a way that the probability of turbulence collapse is very small for small Ri, but increases to virtual certainty for sufficiently large Ri. The presence of such a transition range in which either regime could be occupied is consistent with the observed overlap of the wSBL and vSBL in the distributions of shear, stratification, and turbulence (AM18a). In the vSBL state, random 'kicks' of TKE can be added as

5   representation of the effects of intermittent turbulent events which erode the stratification and reduce Ri. With a Ri dependent $P(\mathrm{vSBL} \rightarrow \mathrm{wSBL})$, after a sufficiently large input of energy, the system will have a high probability of transitioning back into the wSBL. We propose a compound Poisson process representation of the random 'kicks' as intermittent turbulence events are associated with many different phenomena (such as breaking gravity waves, density currents etc.) which are independent from each other and can produce very different turbulence intensities. Such a parameterisation can account for the observed

10   non-Markov recovery time between transitions as after entering the wSBL state a certain time is required to build up the stratification so that a transition to the vSBL occurs, and in the vSBL time is required for intermittent turbulence kicks to sufficiently erode the stratification and result in the reverse transition. Furthermore, this picture is consistent with the observed enhancement of TKE values before a vSBL to wSBL transition and with the relatively gradual decay of turbulence across the wSBL to vSBL transition (AM18c). The fact that event duration distributions are very similar between the tower sites suggests that

15   the compound Poisson process can be parameterised independent of the local complexity of the surface conditions (such as surface type, topography etc.)

The observational information on climatological regime statistics, and event duration distributions (cf. AM18b, AM18c, and the present study) can then be used to tune the parameterisation to generate the appropriate SBL regime variability. The results obtained for stationary Markov chain average persistence probabilities in this study can be used to constrain the average

20   behaviour of the state-dependent persistence probabilities. The fact that no set of persistence probabilities allows the stationary Markov chain to produce both the observed very persistent night statistics and transition statistics suggests that some compromise between these two might be necessary (although the extra freedom provided by the state-dependent transition probabilities may result in better simulations of both sets of regime statistics than was possible by the stationary Markov chain).

Finally, the development of such a parameterisation requires further information regarding horizontal dependence of regime

25   statistics, as it is not reasonable to expect an entire large-scale weather or climate model grid box to always be in one or the other state. This horizontal dependence will be the subject of a future study. Assessment of the dependence length scales relative to the grid box size will allow the determination of to what extent the subgrid-scale variability can be represented by a deterministic average, or if its parameterisation must be explicitly stochastic.

Appendix A

30   In this appendix, we present the calculations of quantities based on stationary Markov chains.

Nonlinear Processes
in Geophysics
Discussions

A1 Calculation of very persistent regimes

The occurrence probability of very persistent SBL nights in a stationary Markov chain is calculated using the persistence probabilities of the Markov chain (i.e. $P(\text{wSBL} \to \text{wSBL})$ and $P(\text{vSBL} \to \text{vSBL})$) as follows

$$Pr(\text{wSBL}|n) \quad = \pi_{\text{wSBL}} P(\text{wSBL} \to \text{wSBL})^n, \tag{A1}$$

$$Pr(\text{vSBL}|n) \quad = \pi_{\text{vSBL}} P(\text{vSBL} \to \text{vSBL})^n. \tag{A2}$$

where π_{wSBL} and π_{vSBL} are respectively the initial climatological distributions of being in the wSBL or vSBL and n equals the length of the night in hours multiplied by six (corresponding to a data resolution of 10 min)

A2 Calculation of at least one particular SBL transition occurrence

The probability of the occurrence of a particular SBL transition in a night of duration n can be expressed in terms of the probability of the absence of any transitions and the probability of single transitions of the complementary transition. In the case of the wSBL to vSBL transition the single complementary transitions start in the vSBL is only allowed a transition to the wSBL. Naturally, the reverse is true for vSBL to wSBL transitions. That way we account for all possibilities that definitely do not have a transition of the considered type.

The probability of the occurrence of turbulence collapse is:

$$Pr((\text{wSBL} \to \text{vSBL}|n) > 0) = 1 - \underbrace{\pi_{\text{wSBL}} P(\text{wSBL} \to \text{wSBL})^n}_{\text{prob. of remaining in the wSBL}}$$

$$- \underbrace{\pi_{\text{vSBL}} P(\text{vSBL} \to \text{vSBL})^n}_{\text{prob. of remaining in the vSBL}} \tag{A3}$$

$$\underbrace{- \sum_{t=0}^{n-1} \pi_{\text{vSBL}} P(\text{vSBL} \to \text{vSBL})^t P(\text{vSBL} \to \text{wSBL}) P(\text{wSBL} \to \text{wSBL})^{n-t-1}}_{\text{prob. of only vSBL to wSBL transitions, remaining in the wSBL afterwards}},$$

Equivalently, the probability of a turbulence recovery (vSBL to wSBL transition) is given by

$$Pr((\text{vSBL} \to \text{wSBL}|n) > 0) = 1 - \underbrace{\pi_{\text{wSBL}} P(\text{wSBL} \to \text{wSBL})^n}_{\text{prob. of remaining in the wSBL}}$$

$$- \underbrace{\pi_{\text{vSBL}} P(\text{vSBL} \to \text{vSBL})^n}_{\text{prob. of remaining in the vSBL}} \tag{A4}$$

$$\underbrace{- \sum_{t=0}^{n-1} \pi_{\text{wSBL}} P(\text{wSBL} \to \text{wSBL})^t P(\text{wSBL} \to \text{vSBL}) P(\text{vSBL} \to \text{vSBL})^{n-t-1}}_{\text{prob. of only wSBL to vSBL transitions, remaining in the vSBL afterwards}}.$$

Nonlinear Processes
in Geophysics

Discussions

Open Access

EGU

A3 Calculation of the probability of subsequent turbulence recovery or collapse event occurrences

The probability that a turbulence recovery event occurs after a turbulence collapse in a night of duration n is equal to the sum of the probabilities of all events that include the occurrence of SBL patterns starting at time t_1 in the wSBL, and afterwards showing the sequence $\mathrm{wSBL} \to \overbrace{\mathrm{vSBL} \to \ldots \to \mathrm{vSBL}}^{t\times} \to \mathrm{wSBL}$ with no further subsequent recovery events, i.e. the SBL

5   remains in the wSBL or have a maximum of one more collapse. The last part of this calculation assures that no double counting of sequences with length t occur as the probability calculation of being in the wSBL at time t_1 does not include information of the preceding path. The probability of a certain subsequent recovery pattern of length t can then be calculated as

$$Pr((\mathrm{wSBL} \to \overbrace{\mathrm{vSBL} \to \ldots \to \mathrm{vSBL}}^{t\times} \to \mathrm{wSBL}|n) > 0) = \sum_{t_1=0}^{n-t-2} (\pi^T \mathbf{Q}^{t_1})_{\mathrm{wSBL}}$$

$$P(\mathrm{wSBL} \to \mathrm{vSBL})P(\mathrm{vSBL} \to \mathrm{vSBL})^t P(\mathrm{vSBL} \to \mathrm{wSBL}) \left[P(\mathrm{wSBL} \to \mathrm{wSBL})^{n-t-t_1-2} \right. \tag{A5}$$

$$\left. + \sum_{t_2=0}^{n-t-t_1-3} P(\mathrm{wSBL} \to \mathrm{wSBL})^{t_2} P(\mathrm{wSBL} \to \mathrm{vSBL})P(\mathrm{vSBL} \to \mathrm{vSBL})^{n-t-t_1-t_2-3} \right],$$

where π is the vector of climatological initial probabilities.

10   To calculate the overall probability that such a subsequent event occurs is then the summation over all possible t:

$$\sum_t Pr((\mathrm{wSBL} \to \overbrace{\mathrm{vSBL} \to \ldots \to \mathrm{vSBL}}^{t\times} \to \mathrm{wSBL}|n) > 0) = \sum_{t=0}^{n-2} \sum_{t_1=0}^{n-t-2} (\pi^T \mathbf{Q}^{t_1})_{\mathrm{wSBL}}$$

$$P(\mathrm{wSBL} \to \mathrm{vSBL})P(\mathrm{vSBL} \to \mathrm{vSBL})^t P(\mathrm{vSBL} \to \mathrm{wSBL}) \left[P(\mathrm{wSBL} \to \mathrm{wSBL})^{n-t-t_1-2} \right. \tag{A6}$$

$$\left. + \sum_{t_2=0}^{n-t-t_1-3} P(\mathrm{wSBL} \to \mathrm{wSBL})^{t_2} P(\mathrm{wSBL} \to \mathrm{vSBL})P(\mathrm{vSBL} \to \mathrm{vSBL})^{n-t-t_1-t_2-3} \right]$$

Equivalently, the probabilities of subsequent turbulence collapses after recovery events are

$$Pr((\mathrm{vSBL} \to \overbrace{\mathrm{wSBL} \to \ldots \to \mathrm{wSBL}}^{t\times} \to \mathrm{vSBL}|n) > 0) = \sum_{t_1=0}^{n-t-2} (\pi^T \mathbf{Q}^{t_1})_{\mathrm{vSBL}}$$

$$P(\mathrm{vSBL} \to \mathrm{wSBL})P(\mathrm{wSBL} \to \mathrm{wSBL})^t P(\mathrm{wSBL} \to \mathrm{vSBL}) \left[P(\mathrm{vSBL} \to \mathrm{vSBL})^{n-t-t_1-2} \right. \tag{A7}$$

$$\left. + \sum_{t_2=0}^{n-t-t_1-3} P(\mathrm{vSBL} \to \mathrm{vSBL})^{t_2} P(\mathrm{vSBL} \to \mathrm{wSBL})P(\mathrm{wSBL} \to \mathrm{wSBL})^{n-t-t_1-t_2-3} \right]$$

To calculate the overall probability that such a subsequent event occurs is then the summation over all possible t:

$$\sum_t Pr((\text{vSBL} \rightarrow \overbrace{\text{wSBL} \rightarrow \dots \rightarrow \text{wSBL}}^{t\times} \rightarrow \text{vSBL}|n) > 0) = \sum_{t=0}^{n-2} \sum_{t_1=0}^{n-t-2} (\pi^T \mathbf{Q}^{t_1})_{\text{vSBL}}$$

$$P(\text{vSBL} \rightarrow \text{wSBL})P(\text{wSBL} \rightarrow \text{wSBL})^t P(\text{wSBL} \rightarrow \text{vSBL})\Bigg[P(\text{vSBL} \rightarrow \text{vSBL})^{n-t-t_1-2} \tag{A8}$$

$$+ \sum_{t_2=0}^{n-t-t_1-3} P(\text{vSBL} \rightarrow \text{vSBL})^{t_2} P(\text{vSBL} \rightarrow \text{wSBL})P(\text{wSBL} \rightarrow \text{wSBL})^{n-t-t_1-t_2-3} \Bigg]$$

Competing interests. The authors declare that they have no conflict of interest.

Nonlinear Processes in Geophysics
Discussions
Open Access
EGU

References

Abraham, C. and Monahan, A. H.: Regimes of the stably stratified nocturnal boundary layer. Part I: Observable meteorological state variables containing information about regime occupation, submitted to J. Atmos. Sci., 2018a.

Abraham, C. and Monahan, A. H.: Regimes of the stably stratified nocturnal boundary layer. Part II: The boundary layer structure in times of very persistent weakly stable and very stable boundary layer conditions, submitted to J. Atmos. Sci., 2018b.

Abraham, C. and Monahan, A. H.: Regimes of the stably stratified nocturnal boundary layer. Part III: The structure of meteorological state variables and the role of external forces in times of regime transitions, submitted to J. Atmos. Sci., 2018c.

Acevedo, O. C. and Fitzjarrald, D. R.: In the Core of the Night-Effects of Intermittent Mixing on a Horizontally Heterogeneous Surface, Bound. Lay. Meteorol., 106, 1–33, https://doi.org/10.1023/A:1020824109575, 2003.

Acevedo, O. C., Moraes, O. L. L., Degrazia, G. A., and Medeiros, L. E.: Intermittency and the Exchange of Scalars in the Nocturnal Surface Layer, Bound. Lay. Meteorol., 119, 41–55, https://doi.org/10.1007/s10546-005-9019-3, 2006.

Acevedo, O. C., Mahrt, L., Puhales, F. S., Costa, F. D., Medeiros, L. E., and Degrazia, G. A.: Contrasting structures between the decoupled and coupled states of the stable boundary layer, Q. J. R. Meteor. Soc., 142, 693–702, https://doi.org/10.1002/qj.2693, 2016.

Ansorge, C. and Mellado, J. P.: Global Intermittency and Collapsing Turbulence in the Stratified Planetary Boundary Layer, Bound. Lay. Meteorol., 153, 89–116, https://doi.org/10.1007/s10546-014-9941-3, 2014.

Baas, P., Bosveld, F. C., Baltink, H. K., and Holtslag, A. A. M.: A Climatology of Nocturnal Low-Level Jets at Cabauw, J. Appl. Meteor. Climatol., 48, 1627–1642, https://doi.org/10.1175/2009JAMC1965.1, 2009.

Barthlott, C., Kalthoff, N., and Fiedler, F.: Influence of high-frequency radiation on turbulence measurements on a 200 m tower, Meteorol. Z, 12, 67–71(5), https://doi.org/10.1127/0941-2948/2003/0012-0067, 2003.

Basu, S., Porté-agel, F., Foufoula-Georgiou, E., Vinuesa, J.-F., and Pahlow, M.: Revisiting the Local Scaling Hypothesis in Stably Stratified Atmospheric Boundary-Layer Turbulence: an Integration of Field and Laboratory Measurements with Large-Eddy Simulations, Bound. Lay. Meteorol., 119, 473–500, https://doi.org/10.1007/s10546-005-9036-2, 2006.

Bechtold, P., Köhler, M., Jung, T., Doblas-Reyes, F., Leutbecher, M., Rodwell, M. J., Vitart, F., and Balsamo, G.: Advances in simulating atmospheric variability with the ECMWF model: From synoptic to decadal time-scales, Quarterly Journal of the Royal Meteorological Society, 134, 1337–1351, https://doi.org/10.1002/qj.289, 2008.

Beeken, A., Neumann, T., and Westerhellweg, A.: Five Years of Operation of the First Offshore Wind Research Platform in the German Bight – FINO1, Tech. rep., German Wind Energy Institute (DEWI GmbH), DEWEK, DEWI GmbH, Ebertstraße 96, D-26382 Wilhelmshaven, article available at: http://www.dewi.de/dewi/fileadmin/pdf/publications/Publikations/5_Beeken.pdf, 2008.

Blumen, W.: An observational study of instability and turbulence in nighttime drainage winds, Bound. Lay. Meteorol., 28, 245–269, https://doi.org/10.1007/BF00121307, 1984.

Blumen, W., Banta, R., Burns, S. P., Fritts, D. C., Newsom, R., Poulos, G. S., and Sun, J.: Turbulence statistics of a Kelvin–Helmholtz billow event observed in the night-time boundary layer during the Cooperative Atmosphere–Surface Exchange Study field program, Dyn. Atmos. Oceans, 34, 189–204, https://doi.org/10.1016/S0377-0265(01)00067-7, 2001.

Bosveld, F. C., Baas, P., Steeneveld, G.-J., Holtslag, A. A. M., Angevine, W. M., Bazile, E., de Bruijn, E. I. F., Deacu, D., Edwards, J. M., Ek, M., Larson, V. E., Pleim, J. E., Raschendorfer, M., and Svensson, G.: The Third GABLS Intercomparison Case for Evaluation Studies of Boundary-Layer Models. Part B: Results and Process Understanding, Bound. Lay. Meteorol., 152, 157–187, https://doi.org/10.1007/s10546-014-9919-1, 2014.

Bowen, B. M., Baars, J. A., and Stone, G. L.: Nocturnal Wind Direction Shear and Its Potential Impact on Pollutant Transport, J. Appl. Meteor. Climatol., 39, 437–445, https://doi.org/10.1175/1520-0450(2000)039<0437:NWDSAI>2.0.CO;2, 2000.

Brümmer, B., Lange, I., and Konow, H.: Atmospheric boundary layer measurements at the 280 m high Hamburg weather mast 1995-2011: mean annual and diurnal cycles, Meteorol. Z., 21, 319–335, https://doi.org/10.1127/0941-2948/2012/0338, 2012.

5   Coulter, R. L. and Doran, J. C.: Spatial and Temporal Occurrences of Intermittent Turbulence During CASES-99, Bound. Lay. Meteorol., 105, 329–349, https://doi.org/10.1023/A:1019993703820, 2002.

Dempster, A. P., Laird, N. M., and Rubin, D. B.: Maximum Likelihood from Incomplete Data via the EM Algorithm, J. Roy. Stat. Soc., 39B, 1–38, 1979.

Dethloff, K., Abegg, C., Rinke, A., Hebestadt, I., and Romanov, V. F.: Sensitivity of Arctic climate simulations to different boundary-layer 10   parameterizations in a regional climate model, Tellus A, 53, 1–26, https://doi.org/10.1034/j.1600-0870.2001.01073.x, 2001.

Donda, J. M. M., van Hooijdonk, I. G. S., Moene, A. F., Jonker, H. J. J., van Heijst, G. J. F., Clercx, H. J. H., and van de Wiel, B. J. H.: Collapse of turbulence in stably stratified channel flow: a transient phenomenon, Quarterly Journal of the Royal Meteorological Society, 141, 2137–2147, https://doi.org/10.1002/qj.2511, http://dx.doi.org/10.1002/qj.2511, 2015.

Doran, J. C.: Characteristics of Intermittent Turbulent Temperature Fluxes in Stable Conditions, Bound. Lay. Meteorol., 112, 241–255, 15   https://doi.org/10.1023/B:BOUN.0000027907.06649.d0, 2004.

Dörenkämper, M., Witha, B., Steinfeld, G., Heinemann, D., and Kühn, M.: The impact of stable atmospheric boundary layers on wind-turbine wakes within offshore wind farms, Journal of Wind Engineering and Industrial Aerodynamics, 144, 146–153, https://doi.org/10.1016/j.jweia.2014.12.011, 2015.

Edwards, J. M., McGregor, J. R., Bush, M. R., and Bornemann, F. J. A.: Assessment of numerical weather forecasts against observations from 20   Cardington: seasonal diurnal cycles of screen-level and surface temperatures and surface fluxes, Q. J. R. Meteorol. Soc., 137, 656–672, https://doi.org/10.1002/qj.742, 2011.

Fischer, J.-G., Senet, C., Outzen, O., Schneehorst, A., and Herklotz, K.: Regional oceanographic distincions in the South-Eastern part of the North Sea: Results of two years of monitoring at the research platforms FINO1 and FINO3, in: German Wind Energy Conference DEWEK 2012, J.-G. Fischer, Ed., Bremen, Germany, 2012, 2012.

25   Floors, R., Peña, A., and Gryning, S.-E.: The effect of baroclinicity on the wind in the planetary boundary layer, Q. J. R. Meteor. Soc., 141, 619–630, https://doi.org/10.1002/qj.2386, 2014.

Flores, O. and Riley, J. J.: Analysis of Turbulence Collapse in the Stably Stratified Surface Layer Using Direct Numerical Simulation, Boundary-Layer Meteorology, 139, 241–259, https://doi.org/10.1007/s10546-011-9588-2, https://doi.org/10.1007/s10546-011-9588-2, 2011.

30   Fu, G., Charles, S. P., and Kirshner, S.: Daily rainfall projections from general circulation models with a downscaling nonhomogeneous hidden Markov model (NHMM) for south-eastern Australia, Hydrological Processes, 27, 3663–3673, https://doi.org/10.1002/hyp.9483, https://onlinelibrary.wiley.com/doi/abs/10.1002/hyp.9483, 2013.

Gerbig, C., Körner, S., and Lin, J. C.: Vertical mixing in atmospheric tracer transport models: error characterization and propagation, Atmos. Chem. Phys., 8, 591–602, https://doi.org/10.5194/acp-8-591-2008, 2008.

35   Gryning, S.-E., Floors, R., Peña, A., Batchvarova, E., and Brümmer, B.: Weibull Wind-Speed Distribution Parameters Derived from a Combination of Wind-Lidar and Tall-Mast Measurements Over Land, Coastal and Marine Sites, Bound. Lay. Meteorol., 159, 329–348, https://doi.org/10.1007/s10546-015-0113-x, 2016.

He, Y., Monahan, A. H., Jones, C. G., Dai, A., Biner, S., Caya, D., and Winger, K.: Probability distributions of land surface wind speeds over North America, Journal of Geophysical Research: Atmospheres, 115, D04 103, https://doi.org/10.1029/2008JD010708, 2010.

He, Y., McFarlane, N. A., and Monahan, A. H.: The Influence of Boundary Layer Processes on the Diurnal Variation of the Climatological Near-Surface Wind Speed Probability Distribution over Land, J. Climate, 115, D04 103, https://doi.org/10.1175/JCLI-D-11-00321.1, 2012.

Holdsworth, A. M., Rees, T., and Monahan, A. H.: Parameterization Sensitivity and Instability Characteristics of the Maximum Sustainable Heat Flux Framework for Predicting Turbulent Collapse, J. Atmos. Sci., 73, 3527–3540, https://doi.org/10.1175/JAS-D-16-0057.1, 2016.

Holtslag, A. A. M., Svensson, G., Baas, P., Basu, S., Beare, B., Beljaars, A. C. M., Bosveld, F. C., Cuxart, J., Lindvall, J., Steeneveld, G. J., Tjernström, M., and Wiel, B. J. H. V. D.: Stable Atmospheric Boundary Layers and Diurnal Cycles: Challenges for Weather and Climate Models, Bull. Amer. Meteor. Soc., 94, 1691–1706, https://doi.org/10.1175/BAMS-D-11-00187.1, 2013.

Hughes, J. P., Guttorp, P., and Charles, S. P.: A non-homogeneous hidden Markov model for precipitation occurrence, Journal of the Royal Statistical Society: Series C (Applied Statistics), 48, 15–30, https://doi.org/10.1111/1467-9876.00136, https://rss.onlinelibrary.wiley.com/doi/abs/10.1111/1467-9876.00136, 1999.

Kaimal, J. C. and Gaynor, J. E.: The Boulder Atmospheric Observatory, J. Appl. Meteor. Climatol., 22, 863–880, https://doi.org/10.1175/1520-0450(1983)022<0863:TBAO>2.0.CO;2, 1983.

Kalthoff, N. and Vogel, B.: Counter-current and channelling effect under stable stratification in the area of Karlsruhe, Theor. Appl. Climatol., 45, 113–126, https://doi.org/10.1007/BF00866400, 1992.

Kyselý, J. and Plavcová, E.: Biases in the diurnal temperature range in Central Europe in an ensemble of regional climate models and their possible causes, Clim. Dyn., 39, 1275–1286, https://doi.org/10.1007/s00382-011-1200-4, 2012.

Lang, F., Belušić, D., and Siems, S.: Observations of Wind-Direction Variability in the Nocturnal Boundary Layer, Bound. Lay. Meteorol., 166, 51–68, https://doi.org/10.1007/s10546-017-0296-4, 2018.

Mahrt, L.: Nocturnal Boundary-Layer Regimes, Bound. Lay. Meteorol., 88, 255–278, https://doi.org/10.1023/A:1001171313493, 1998a.

Mahrt, L.: Stratified atmospheric boundary layers and breakdown of models, Theor. Comput. Fluid Phys., 11, 263–279, https://doi.org/10.1007/s001620050093, 1998b.

Mahrt, L.: Common microfronts and other solitary events in the nocturnal boundary layer, Q. J. R. Meteor. Soc., 136, 1712–1722, https://doi.org/10.1002/qj.694, 2010.

Mahrt, L.: Stably Stratified Atmospheric Boundary Layers, Annu. Rev. Fluid Mech., 46, 23–45, https://doi.org/10.1146/annurev-fluid-010313-141354, 2014.

Mauritsen, T. and Svensson, G.: Observations of Stably Stratified Shear-Driven Atmospheric Turbulence at Low and High Richardson Numbers, J. Atmos. Sci., 64, 645–655, https://doi.org/10.1175/JAS3856.1, 2007.

Medeiros, B., Deser, C., Tomas, R. A., , and Kay, J. E.: Arctic inversion strength in climate models, J. Climate, 24, 4733–4740, https://doi.org/10.1175/2011JCLI3968.1, 2011.

Monahan, A. H., He, Y., McFarlane, N., and Dai, A.: The Probability Distribution of Land Surface Wind Speeds, J. Climate, 24, 3892–3909, https://doi.org/10.1175/2011JCLI4106.1, 2011.

Monahan, A. H., Rees, T., He, Y., and McFarlane, N.: Multiple Regimes of Wind, Stratification, and Turbulence in the Stable Boundary Layer, J. Atmos. Sci., 72, 3178–3198, https://doi.org/10.1175/JAS-D-14-0311.1, 2015.

Nappo, C., Sun, J., Mahrt, L., and ić, D. B.: Determining Wave–Turbulence Interactions in the Stable Boundary Layer, Bull. Amer. Meteor. Soc., 95, ES11–ES13, https://doi.org/10.1175/BAMS-D-12-00235.1, 2014.

Nappo, C. J.: Sporadic breakdowns of stability in the PBL over simple and complex terrain, Bound. Lay. Meteorol., 54, 69–87, https://doi.org/10.1007/BF00119413, 1991.

Newsom, R. K. and Banta, R. M.: Shear-Flow Instability in the Stable Nocturnal Boundary Layer as Observed by Doppler Lidar during CASES-99, J. Atmos. Sci., 60, 16–33, https://doi.org/10.1175/1520-0469(2003)060<0016:SFIITS>2.0.CO;2, 2003.

5   O'Brien, T. A., D.Collins, W., A.Rauscher, S., and D.Ringler, T.: Reducing the computational cost of the ECF using a nuFFT: A fast and objective probability density estimation method, Comput. Stat. Data Anal., 79, 222–234, https://doi.org/10.1016/j.csda.2014.06.002, 2014.

O'Brien, T. A., Kashinath, K., Cavanaugh, N. R., D.Collins, W., and O'Brien, J. P.: A fast and objective multidimensional kernel density estimation method: fastKDE, Comput. Stat. Data Anal., 101, 148–160, https://doi.org/10.1016/j.csda.2016.02.014, 2016.

Prabha, T., Hoogenboom, G., and Smirnova, T.: Role of land surface parameterizations on modeling cold-pooling events and low-level jets,
10   Atmos. Res., 99, 147–161, https://doi.org/10.1016/j.atmosres.2010.09.017, 2011.

Rabiner, L. R.: A tutorial on hidden Markov models and selected applications in speech recognition, Proc. IEEE, 77, 257–286, https://doi.org/10.1109/5.18626, 1989.

Rees, J. M. and Mobbs, S. D.: Studies of internal gravity waves at Halley Base, Antarctica, using wind observations, Q. J. R. Meteor. Soc., 114, 939–966, https://doi.org/10.1002/qj.49711448206, 1988.

15   Rishel, J., Johnson, S., and Holt, D.: Meteorological monitoring at Los Alamos. Los Alamos National Progress Report LA-UR-03-9097, Tech. rep., Los Alamos National Laboratory, available at: http://environweb.lanl.gov/downloads/LA-UR-03-8097_webcopy.pdf, 2003.

Salmond, J. A. and McKendry, I. G.: A review of turbulence in the very stable nocturnal boundary layer and its implications for air quality, Progress in Physical Geography, 29, 171–188, https://doi.org/10.1191/0309133305pp442ra, 2005.

Sterk, H. A. M., Steeneveld, G. J., and Holtslag, A. A. M.: The role of snow-surface coupling, radiation, and turbulent mixing in modeling a
20   stable boundary layer over Arctic sea ice, J. Geophys. Res. Atmos., 118, 1199–1217, https://doi.org/10.1002/jgrd.50158, 2013.

Sterk, H. A. M., Steeneveld, G. J., Vihma, T., Anderson, P. S., Bosveld, F. C., and Holtslag, A. A. M.: Clear-sky stable boundary layers with low winds over snow-covered surfaces. Part 1: WRF model evaluation, Quarterly Journal of the Royal Meteorological Society, 141, 2165–2184, https://doi.org/10.1002/qj.2513, http://dx.doi.org/10.1002/qj.2513, 2015.

Storm, B. and Basu, S.: The WRF Model Forecast-Derived Low-Level Wind Shear Climatology over the United States Great Plains, Energies,
25   3, 258–276, https://doi.org/10.3390/en3020258, 2010.

Sun, J., Burns, S. P., Lenschow, D. H., Banta, R., Newsom, R., Coulter, R., Frasier, S., Ince, T., Nappo, C., Cuxart, J., Blumen, W., Lee, X., and Hu, X.-Z.: Intermittent Turbulence Associated with a Density Current Passage in the Stable Boundary Layer, Bound. Lay. Meteorol., 105, 199–219, https://doi.org/10.1023/A:1019969131774, 2002.

Sun, J., Lenschow, D. H., Burns, S. P., Banta, R. M., Newsom, R. K., Coulter, R., Frasier, S., Ince, T., Nappo, C., Balsley, B. B., Jensen,
30   M., Mahrt, L., Miller, D., and Skelly, B.: Atmospheric Disturbances that Generate Intermittent Turbulence in Nocturnal Boundary Layers, Bound. Lay. Meteorol., 110, 255–279, https://doi.org/10.1023/A:1026097926169, 2004.

Sun, J., Mahrt, L., Banta, R. M., and Pichugina, Y. L.: Turbulence Regimes and Turbulence Intermittency in the Stable Boundary Layer during CASES-99, J. Atmos. Sci., 69, 338–351, https://doi.org/10.1175/JAS-D-11-082.1, 2012.

Sun, J., Mahrt, L., Nappo, C., and Lenschow, D. H.: Wind and Temperature Oscillations Generated by Wave–Turbulence Interactions in the
35   Stably Stratified Boundary Layer, J. Atmos. Sci., 72, 1484–1503, https://doi.org/10.1175/JAS-D-14-0129.1, 2015.

Svensson, G. and Holtslag, A. A. M.: Analysis of model results for the turning of the wind and related momentum fluxes in the stable boundary layer, Bound. Lay. Meteorol., 132, 261–277, https://doi.org/10.1007/s10546-009-9395-1, 2009.

Tastula, E.-M., Vihma, T., and Andreas, E. L.: Evaluation of Polar WRF from modeling the atmospheric boundary layer over antarctic sea ice in autumn and winter, Mon. Wea. Rev., 140, 3919–3935, https://doi.org/10.1175/MWR-D-12-00016.1, 2012.

Tomas, J. M., Pourquie, M. J. B. M., and Jonker, H. J. J.: Stable Stratification Effects on Flow and Pollutant Dispersion in Boundary Layers Entering a Generic Urban Environment, Boundary-Layer Meteorology, pp. 159–221, https://doi.org/10.1007/s10546-015-0124-7, 2016.

5 Ulden, A. P. V. and Wieringa, J.: Atmospheric boundary layer research at Cabauw, Bound. Lay. Meteorol., 78, 39–69, https://doi.org/10.1007/BF00122486, 1996.

van de Wiel, B. J. H., Moene, A. F., Steeneveld, G. J., Hartogensis, O. K., and Holtslag, A. A. M.: Predicting the Collapse of Turbulence in Stably Stratified Boundary Layers, Flow, Turbulence and Combustion, 79, 251–274, https://doi.org/10.1007/s10494-007-9094-2, 2007.

van de Wiel, B. J. H., Vignon, E., Baas, P., van Hooijdonk, I. G. S., van der Linden, S. J. A., van Hooft, J. A., Bosveld, F. C., de Roode, S. R.,

10   Moene, A. F., and Genthonc, C.: Regime Transitions in Near-Surface Temperature Inversions: A Conceptual Model, J. Atmos. Sci., 74, 1057–1073, https://doi.org/10.1175/JAS-D-16-0180.1, 2017.

van Hooijdonk, I., Moene, A., Scheffer, M., Clercx, H., and van de Wiel, B.: Early Warning Signals for Regime Transition in the Stable Boundary Layer : A Model Study, Bound. Lay. Meteorol., 162, 283–306, https://doi.org/10.1007/s10546-016-0199-9, 2017.

van Hooijdonk, I. G. S., Donda, J. M. M., Bosveld, H. J. H. C. F. C., and van de Wiel, B. J. H.: Shear Capacity as Prognostic for Nocturnal

15   Boundary Layer Regimes, J. Atmos. Sci., 72, 1518–1532, https://doi.org/10.1175/JAS-D-14-0140.1, 2015.

Vercauteren, N. and Klein, R.: A Clustering Method to Characterize Intermittent Bursts of Turbulence and Interaction with Submesomotions in the Stable Boundary Layer, J. Atmos. Sci., 72, 1504–1517, https://doi.org/10.1175/JAS-D-14-0115.1, 2015.

Vignon, E., van de Wiel, B. J. H., van Hooijdonk, I. G. S., Genthon, C., van der Linden, S. J. A., van Hooft, J. A., Baas, P., Maurel, W., Traullé, O., and Casasanta, G.: Stable boundary-layer regimes at Dome C, Antarctica: observation and analysis, Q. J. R. Meteor. Soc.,

20   143, 1241–1253, https://doi.org/10.1002/qj.2998, 2017.

Walsh, J. E., Chapman, W. L., Romanovsky, V., Christensen, J. H., and Stendel, M.: Global Climate Model Performance over Alaska and Greenland, J. Climate, 21, 6156–6174, https://doi.org/10.1175/2008JCLI2163.1, 2008.

Walters, J. T., McNider, R. T., Shi, X., Norris, W. B., and Christy, J. R.: Positive surface temperature feedback in the stable nocturnal boundary layer, Geophysical Research Letters, 34, L12 709, https://doi.org/10.1029/2007GL029505, 2007.

25 Wenzel, A., Kalthoff, N., and Horlacher, V.: On the profiles of wind velocity in the roughness sublayer above a coniferous forest, Bound. Lay. Meteorol., 84, 219–230, https://doi.org/10.1023/A:1000444911103, 1997.

Westerhellweg, A. and Neumann, T.: FINO1 Mast Correction, DEWI Magazin, 40, 60–66, 2012.

Williams, A. G., Chambers, S., and Griffiths, A.: Bulk Mixing and Decoupling of the Nocturnal Stable Boundary Layer Characterized Using a Ubiquitous Natural Tracer, Bound. Lay. Meteorol., 149, 381–402, https://doi.org/10.1007/s10546-013-9849-3, 2013.

30 Zhou, B. and Chow, F. K.: Turbulence Modeling for the Stable Atmospheric Boundary Layer and Implications for Wind Energy, Flow, Turbulence and Combustion, 88, 255–277, https://doi.org/10.1007/s10494-011-9359-7, 2012.

Zilitinkevich, S. S., Elperin, T., Kleeorin, N., Rogachevskii, I., Esau, I., Mauritsen, T., and Miles, M. W.: Turbulence energetics in stably stratified geophysical flows: Strong and weak mixing regimes, Q. J. R. Meteor. Soc., 134, 793–799, https://doi.org/10.1002/qj.264, 2008.
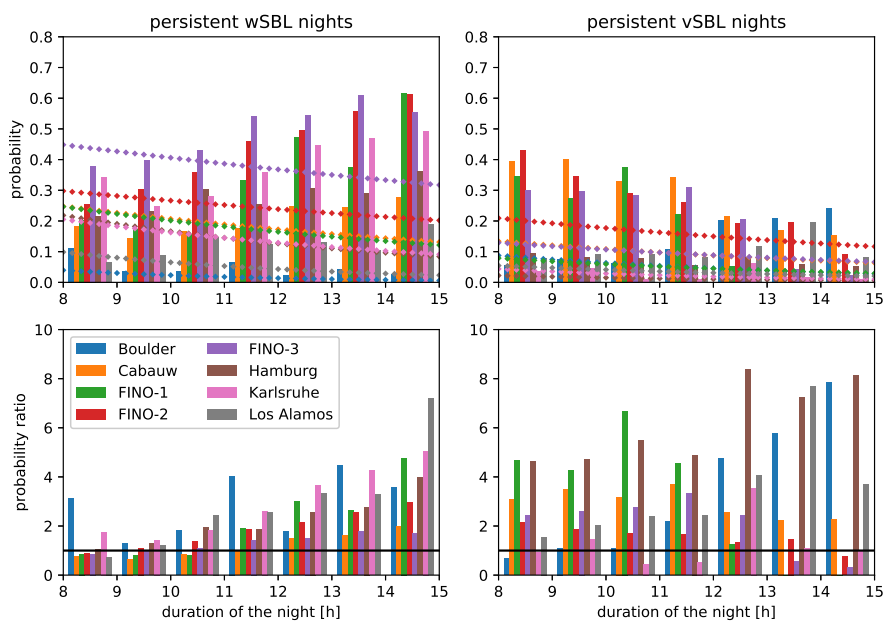
Figure 1. Occurrence probabilities of very persistent wSBL (upper left panel, bars) and vSBL (upper right panel, bars) from the for nights of different lengths (in one hour increments) at the different tower sites compared to the occurrence probabilities of very persistent nights computed from the stationary Markov chain (diamonds). Lower panels show the ratio the probabilities in the upper panels (observed values divided by those from the stationary Markov chain).
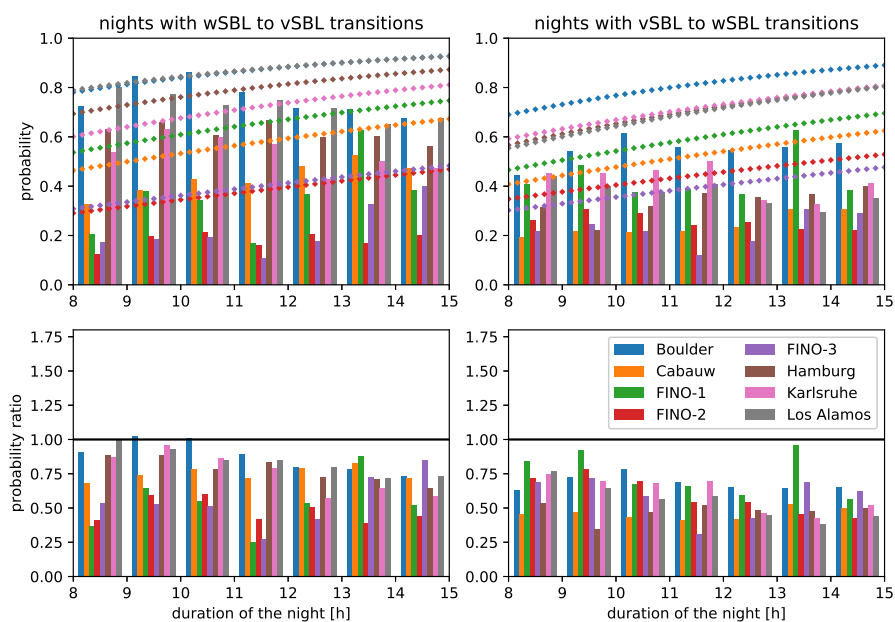
Figure 2. As in Figure 11 but for the occurrence probabilities of wSBL to vSBL (upper left panel) and vSBL and wSBL (upper right panel) transitions.
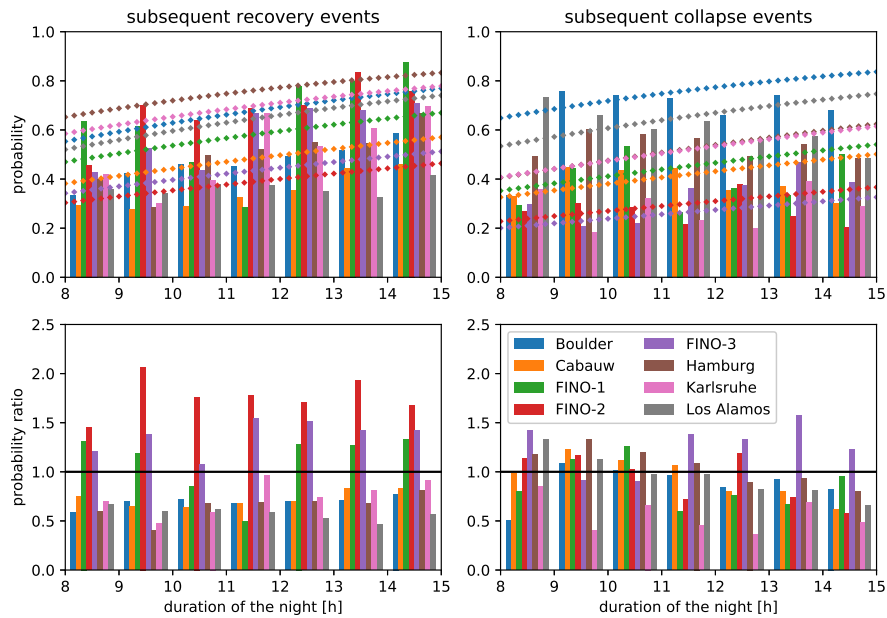
Figure 3. As in Figure 11, but for the probabilities of the occurrence of turbulence recovery events subsequent to turbulence collapse (upper left panel) and turbulence collapse events subsequent to turbulence recovery (upper right panel).
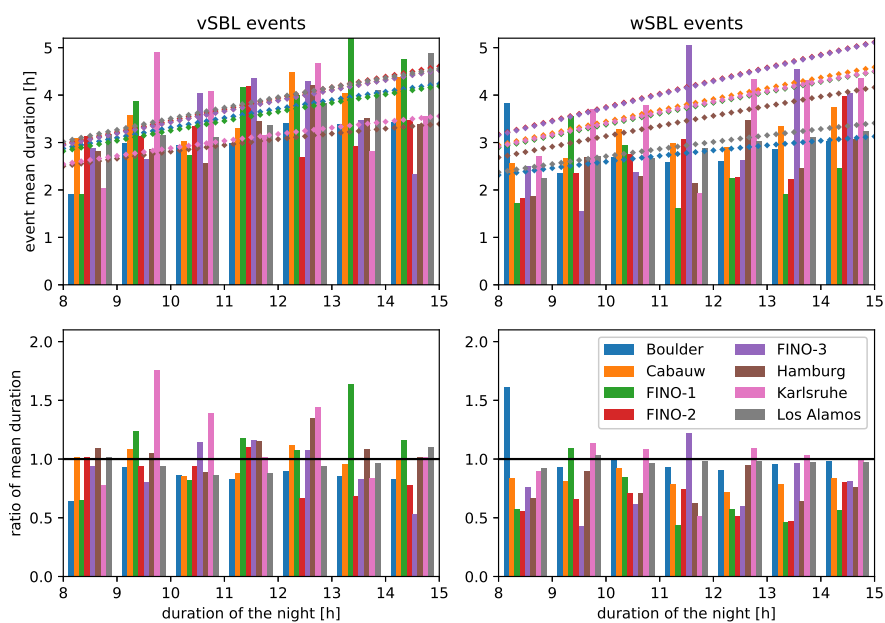
Figure 4. As in Figure 11, but for the mean event duration in the vSBL (upper left panel, bars) in the wSBL (upper right panel, bars).
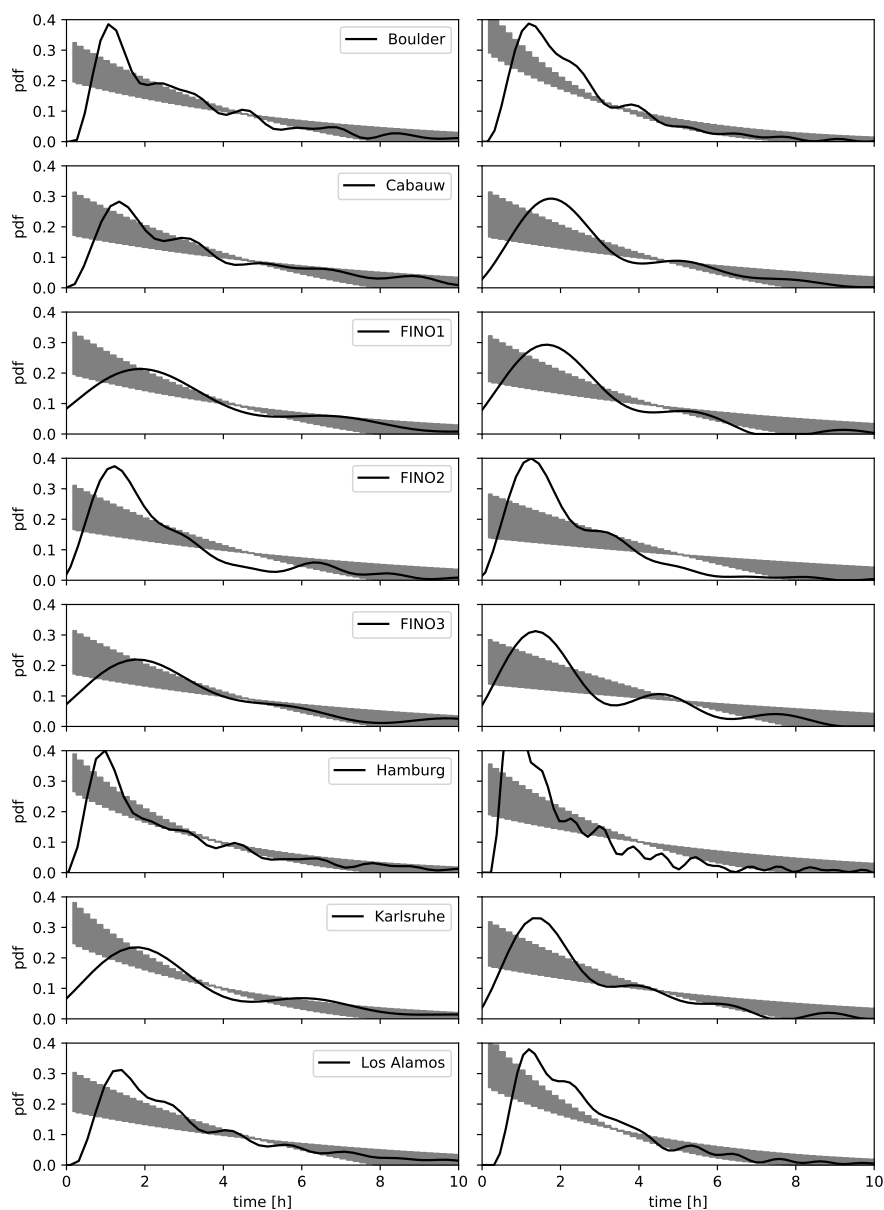
Figure 5. Probability density function of the vSBL events (left panels) and wSBL events (right panels) at the different tower sites. Black lines represent the observed event durations as determined by the HMM analyses and the grey bands denote the pdfs estimated from the stationary Markov chain for nights lasting 8 to 16 hours. All pdfs are calculated with the multivariate kernel density estimation by O'Brien et al. (2014, 2016).
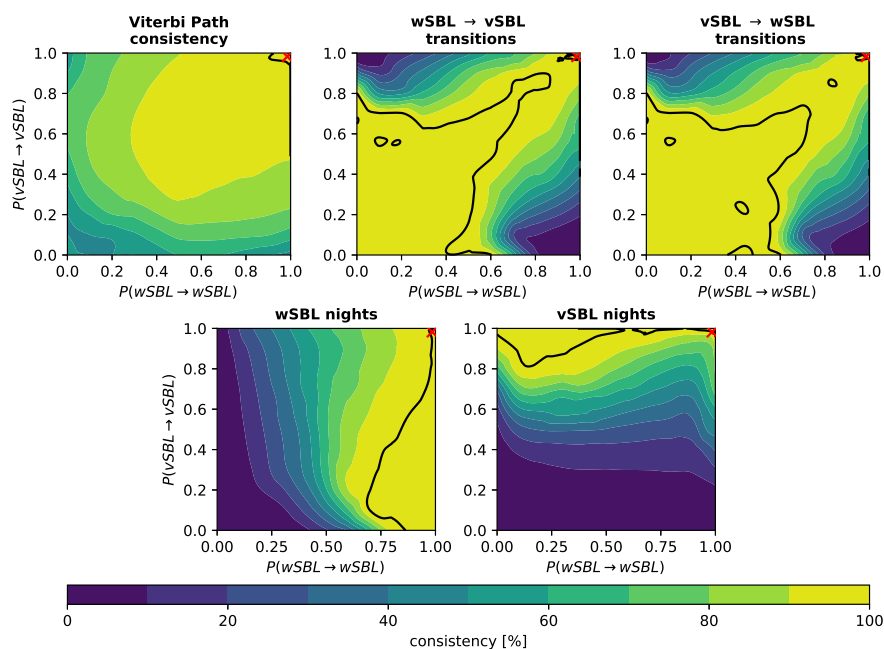
Figure 6. Consistency of reference and perturbed regime occupation statistics as functions of Markov chain persistence probabilities. Displayed are: the overall consistency of the VP (upper left), the consistency of wSBL to vSBL (upper middle) and vSBL to wSBL (upper right) transitions in the VP, the consistency of the occurrence of persistent wSBL (lower left) and vSBL (lower right) nights. In each panel the reference value at Cabauw is shown by a red cross. The 99 % consistency values in each VP characteristic is delineated by a black line.
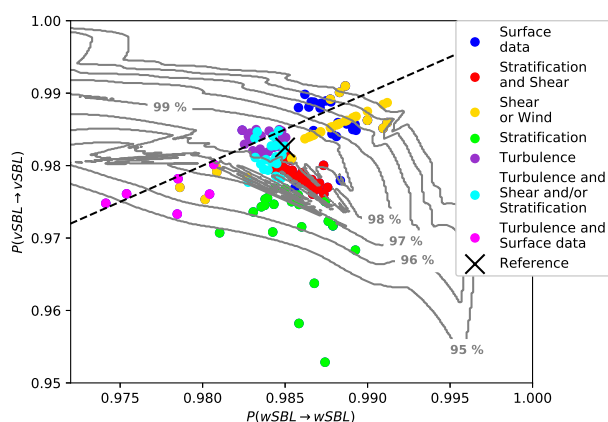
Figure 7. Grey contours: isolines of the total consistency of the perturbed and reference VP (ranges of persistence probabilities where the general VP, transition accuracies, and the accuracy in the occurrence of persistent wSBL and vSBL nights have the same or higher consistencies with the reference VP) at Cabauw. Persistence probabilities estimated from other state variable sets at different observational heights than used in $\mathbf{Y}_{\mathrm{ref}}$ are depicted by coloured dots.
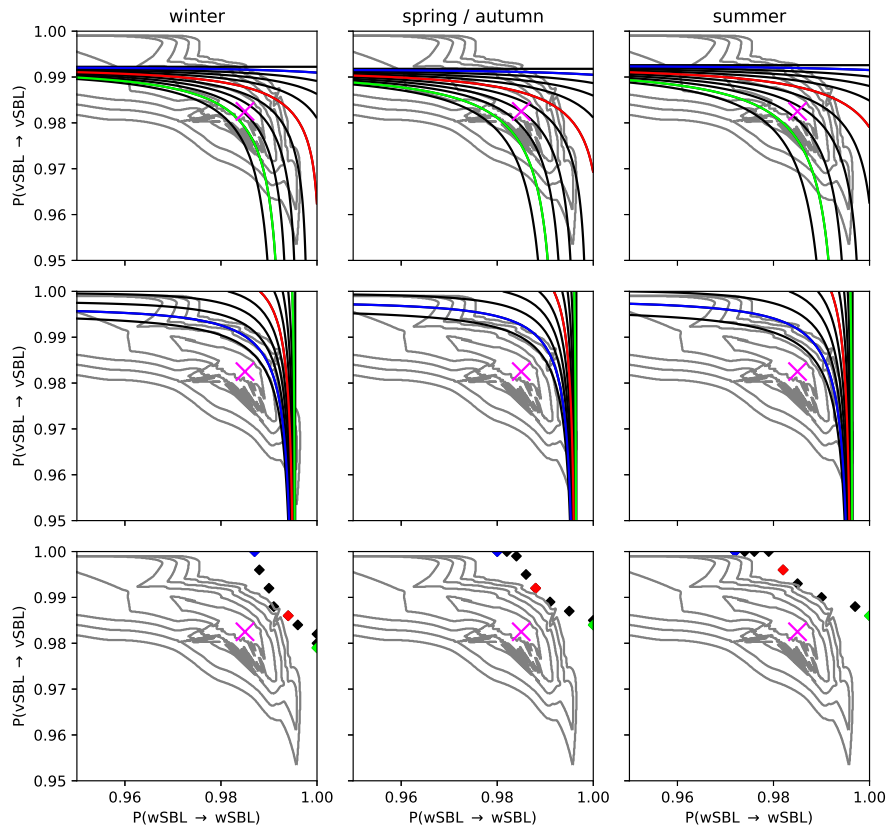
Figure 8. Curves of persistence probabilities yielding stationary Markov chain occurrence probabilities of a at least one wSBL to vSBL (turbulence collapse, top row) and reverse transitions (turbulence recovery, middle row) equal to the observed values, for a range of initial state probabilities π_{wSBL} in 10 % intervals ranging from 0 % to 100 % (10 % in green, 50 % in red, and 90 % in blue) at Cabauw. The bottom row illustrates in the same colour coding the persistence probabilities producing the observational occurrence probability of very persistent wSBL and vSBL nights in a stationary Markov chain. The persistence probability values denoting 95 to 99 % total consistency levels of the perturbed VP with VP_{ref} are depicted in grey contours. The persistence probabilities corresponding to $\mathbf{Q}_{\text{ref}}$ value are marked by a pink cross.
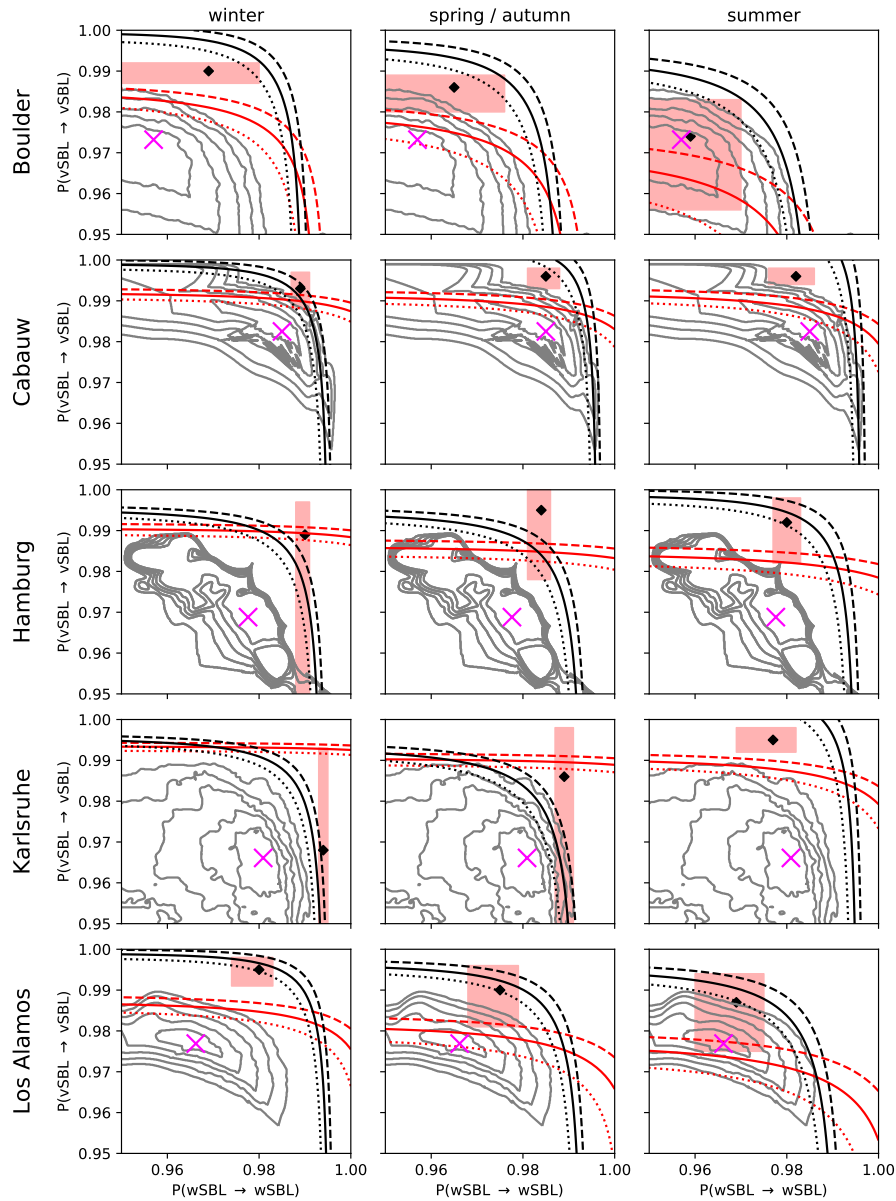
Figure 9. Values of persistence probabilities for which the occurrence probability of at least one wSBL to vBSL transition (turbulence collapse) in a night (red lines) or one vSBL to wSBL (turbulence recovery) in a night (black lines) as computed from a stationary Markov chain equal the observed values. Solid, dashed, and dotted lines correspond respectively the observed values, a probability 5 % below the observed values and a probability 5 % above the observed values. The ranges of persistence probabilities where the occurrence probability of very persistent nights in a stationary Markov chain agrees with observations in a ± 5 % uncertainty band is depicted by the red rectangle with a diamond displaying the values for the exact observational probability occurrence of persistent nights. The persistence probabilities values corresponding to 95 to 99 % total consistency of the perturbed VP with VP$_{\mathrm{ref}}$ in the HMM analysis are depicted in grey contours. The persistence probabilities corresponding to $\mathbf{Q}_{\mathrm{ref}}$ value are marked by a pink cross.
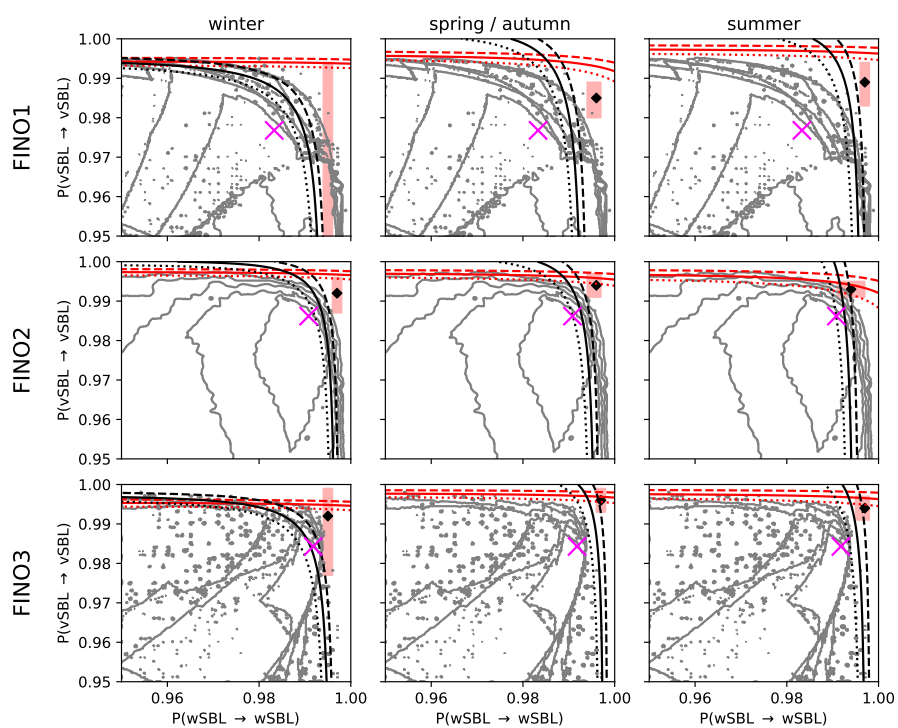
Figure 10. As Figure 19 only for ocean-based stations.

Table 1. Basic information about the different land- and ocean-based tower sites (geographical coordinates, time resolution) and their individual reference HMM state variable inputs $\mathbf{Y}$ (wind speeds W_h and static stabilities $\Delta\Theta$ with their observational levels h) and reference transition probability matrices ($\mathbf{Q}_{\mathrm{ref}}$) of HMM analyses estimated from $\mathbf{Y}$. Starting regimes for the transition probability matrices are denoted with a star. Transition probability matrices at Hamburg and Los Alamos are transformed to a 10 minute time resolution, so a direct comparison to other sites is possible. To retrieve original transition probability matrices at these sites the 1/10 and 3/2 matrix powers (respectively) must be taken.

Tower site	Reference state variables	$\mathbf{Q}_{\mathrm{ref}}$			References
Land-based tower sites					
Boulder	$\mathbf{Y} = (W_{100} - W_{10},$		*wSBL*	*vSBL*	Kaimal and Gaynor (1983),
40.0500 N, 105.0038 W, 1584 m	$0.5(W_{100} + W_{10}),$	*wSBL**	0.9570	0.0430	Blumen (1984)
2008–2015 (10 minute)	$\Theta_{100} - \Theta_{10})$	*vSBL**	0.0268	0.9732	
Cabauw	$\mathbf{Y} = (W_{200} - W_{10},)$		*wSBL*	*vSBL*	Ulden and Wieringa (1996)
51.9700 N, 4.9262 E, -0.7 m	$0.5(W_{200} + W_{10}),$	*wSBL**	0.9850	0.0150	
2001–2015 (10 minute)	$\Theta_{200} - \Theta_2)$	*vSBL**	0.0175	0.9825	
Hamburg	$\mathbf{Y} = (W_{250} - W_{10},$		*wSBL*	*vSBL*	Brümmer et al. (2012),
53.5192 N, 10.1051 E, 0.3 m	$0.5(W_{250} + W_{10}),$	*wSBL**	0.9776	0.0224	Floors et al. (2014),
2005–2015 (1 minute)	$\Theta_{250} - \Theta_2)$	*vSBL**	0.0312	0.9688	Gryning et al. (2016)
Karlsruhe	$\mathbf{Y} = (W_{200} - W_2,$		*wSBL*	*vSBL*	Kalthoff and Vogel (1992),
49.0925 N, 8.4258 E, 110.4 m	$0.5(W_{200} + W_2),$	*wSBL**	0.9809	0.0191	Wenzel et al. (1997),
2003–2013 (10 minute)	$\Theta_{200} - \Theta_2)$	*vSBL**	0.0339	0.9661	Barthlott et al. (2003)
Los Alamos	$\mathbf{Y} = (W_{92} - W_{11.5},$		*wSBL*	*vSBL*	Bowen et al. (2000),
35.8614 N, 106.3196 W, 2263 m	$0.5(W_{92} + W_{11.5}),$	*wSBL**	0.9662	0.0338	Rishel et al. (2003)
1995–2015 (15 minute)	$\Theta_{92} - \Theta_{1.2})$	*vSBL**	0.0231	0.9769	
Ocean-based tower sites					
FINO-1	$\mathbf{Y} = (W_{100} - W_{33},$		*wSBL*	*vSBL*	Beeken et al. (2008),
54.0140 N, 6.5876 E, 0 m	$0.5(W_{100} + W_{33}),$	*wSBL**	0.9833	0.0167	Fischer et al. (2012)
2004–2015 (10 minute)	$\Theta_{100} - \Theta_{30})$	*vSBL**	0.0232	0.9768	
FINO-2	$\mathbf{Y} = (W_{102} - W_{32},$		*wSBL*	*vSBL*	Dörenkämper et al. (2015)
55.0069 N, 13.1542 E, 0 m	$0.5(W_{102} + W_{33}),$	*wSBL**	0.9908	0.0092	
2008–2015 (10 minute)	$\Theta_{99} - \Theta_{30})$	*vSBL**	0.0138	0.9862	
FINO-3	$\mathbf{Y} = (W_{100} - W_{30},$		*wSBL*	*vSBL*	Fischer et al. (2012)
55.1950 N, 7.1583 E, 0 m	$0.5(W_{100} + W_{30}),$	*wSBL**	0.9918	0.0082	
2010–2015	$\Theta_{95} - \Theta_{29})$	*vSBL**	0.0157	0.9843	

Nonlinear Processes
in Geophysics
Discussions

Open Access

EGU

Table 2. Nighttime durations (d) for the different seasons and corresponding average durations for Markov chain calculations.

Season	Observational duration [h]	Markov chain [h]
winter	$13 \leq d$	14
spring / autumn	$11 \leq d \leq 13$	12
summer	$d \leq 11$	10

Nonlinear Processes
in Geophysics
Discussions

Open Access

EGU

Table 3. Probabilities of the occurrence of a wSBL to vSBL (turbulence collapse) or reverse transition (turbulence recovery) in a night, of the occurrence of very persistent wSBL or vSBL nights, and of the climatological initial distributions of starting a night in the wSBL or vSBL (respectively π_{wSBL} and π_{vSBL}) at the different tower sites for different seasons.

Tower station	season	Observations					
		Turbulence		Very persistent		clim.	
		collapse [%]	recovery [%]	wSBL nights [%]	vSBL nights [%]	π_{wSBL}[%]	π_{vSBL} [%]
Land-based stations							
Boulder	winter	68.95	56.5	3.22	22.94	45.59	54.41
	spring / autumn	74.84	55.18	4.44	15.43	56.24	43.76
	summer	82.07	54.41	5.32	7.29	65.2	34.8
Cabauw	winter	48.03	31.69	29.22	14.87	73.44	26.56
	spring / autumn	44.75	22.37	21.36	27.68	63.16	36.84
	summer	35.99	19.1	16.49	38.92	50.50	49.50
Hamburg	winter	54.58	38.78	37.25	5.01	87.36	12.64
	spring / autumn	63.16	36.26	28.36	7.02	89.77	10.23
	summer	59.94	22.86	24.89	10.81	82.22	17.78
Karlsruhe	winter	38.41	31.49	58.13	0.69	95.85	4.15
	spring / autumn	49.45	41.76	40.66	3.85	89.56	10.44
	summer	40.96	22.5	13.85	32.18	57.23	42.77
Los Alamos	winter	65.16	30.95	13.24	16.88	74.41	25.59
	spring / autumn	72.99	36.92	12.86	10.13	79.46	20.54
	summer	74.32	38.57	11.73	9.58	78.75	21.25
Ocean-based stations							
FINO-1	winter	37.84	37.84	62.16	0.00	91.89	8.11
	spring / autumn	23.64	38.18	38.18	16.36	52.73	47.27
	summer	13.64	18.73	56.73	16.91	67.64	32.36
FINO-2	winter	18.93	23.33	58.89	12.81	75.72	24.28
	spring / autumn	18.12	24.83	47.65	22.82	64.77	35.23
	summer	15.1	26.72	28.2	40.19	39.75	60.25
FINO-3	winter	31.56	29.51	57.38	6.97	86.48	13.52
	spring / autumn	14.08	14.79	54.23	26.06	66.2	33.80
	summer	12.23	14.61	50.32	27.16	61.36	38.64